DEVELOPMENT OF A METHOD TO VALIDATE AGRONOMIC DROUGHT AS ASSESSED BY NDVI TIME SERIES THROUGH SATELLITE DERIVED ESTIMATES OF RAINFALL

LAURA GARCÍA VÉLEZ

June, 2016

SUPERVISORS:
Dr. Ir. C.A.J.M de Bie
Dr. B.H.P. Ben Maathuis

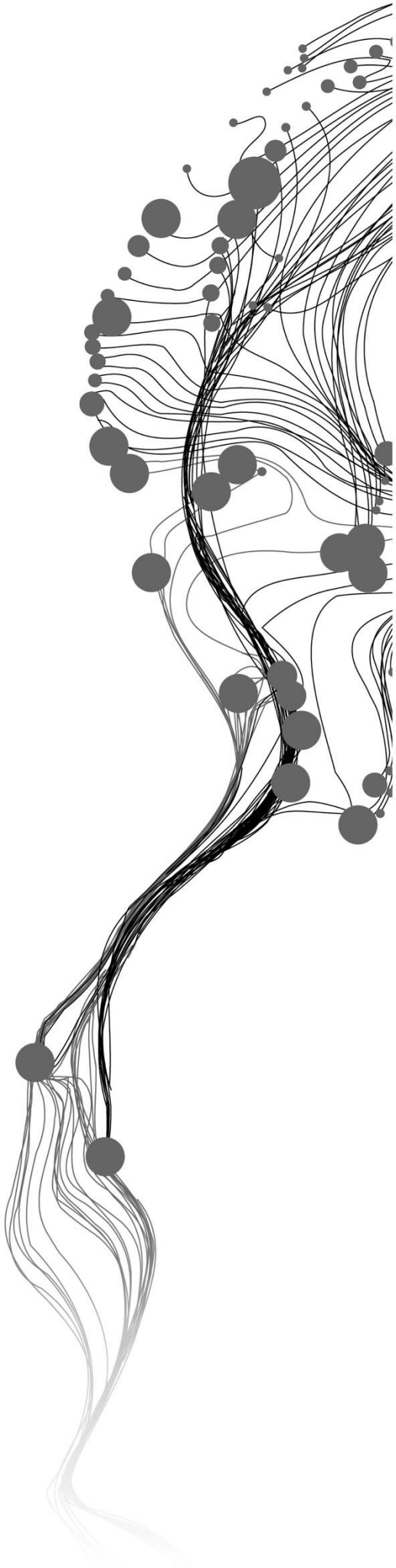

DEVELOPMENT OF A METHOD TO VALIDATE AGRONOMIC DROUGHT AS ASSESSED BY NDVI TIME SERIES THROUGH SATELLITE DERIVED ESTIMATES OF RAINFALL

LAURA GARCÍA VÉLEZ
Enschede, The Netherlands, June, 2016

Thesis submitted to the Faculty of Geo-Information Science and Earth Observation of the University of Twente in partial fulfilment of the requirements for the degree of Master of Science in Geo-information Science and Earth Observation.
Specialization: Geo-information Science and Earth Observation for Environmental Modelling and Management

SUPERVISORS:
Dr. Ir. C.A.J.M de Bie
Dr. B.H.P. Ben Maathuis

THESIS ASSESSMENT BOARD:
Prof. Dr. A.K. Skidmore (Chair), ITC, The Netherlands
Dr. Ir. C.M.M. Mannaerts (External Examiner) ITC, The Netherlands
Dr. Ir. C.A.J.M de Bie (1st supervisor) ITC, The Netherlands
Dr. B.H.P. Ben Maathuis (2nd supervisor) ITC, The Netherlands

ABSTRACT

Considering that the agronomic sector in Ethiopia is highly threatened by drought events, different risk management strategies as weather insurance products have been promoted during the last years. In this context, the use of satellite information is promising as it provides measurements which are spatially continuous and with high temporal resolution.

The GIACIS model (Geodata for Innovative Agricultural Credit Insurance Schemes) uses the Normalize Difference Vegetation Index (NDVI) as a proxy to monitor the occurrence of agronomic drought events. Considering potential limitations of this model to accurately identify the affected areas, the present study explore options of validation through the use of satellite derived estimates of rainfall (meteorological drought). In detail, the validation is carried out over specific Crop Production System Zones (CPS) and its associated growing calendars, using the concept of effective rainfall (available water after losses due to evaporation, deep percolation and runoff). The datasets used are 10-day SPOT-VGT (NDVI) and 10-day CHIRPS (rainfall) imagery.

At first, the study involves; i) derivation of the optimal long term NDVI-rainfall relationships at selected CPS using moving average and Pearson correlation, and ii) improvements in the annual NDVI-rainfall relationship to account for effective rainfall at the region of Tigray (CPS-7) using fixed thresholds. As a result, i) the long term relationships and associated optimal lags portray the general variability that exist among the selected CPS due to the different macro-scale factors that determine the availability of water (e.g. climate, land cover, management practices and soils), and ii) the annual NDVI-effective rainfall relationship of the CPS-7 displays high variability at the end of the growing season, which might be related with other environmental factors that might have higher influence than rainfall during this period, or the need of more refinement in the estimation of effective rainfall.

In this study, the exploration of agreement between agronomic and meteorological drought for the CPS-7 considers the above findings and involves; i) calculation of NDVI and rainfall anomalies through the threshold level method for the years 1999-2014 (CPS level), and ii) Kappa analysis of the spatial agreement between NDVI and rainfall anomalies (pixel level, using a categorical classification). As a result, i) the NDVI and rainfall anomalies agree for 13 out of 16 years in a general linear relationship, ii) the spatial agreement between the anomaly categories is only 21.5% better than chance, which points out that still there are a lot of limitations in the accurate representation of effective rainfall through the use of satellite estimates.

To finalize, the study explores the agreement between agronomic drought (NDVI anomalies) and modelled soil moisture estimates at a selected pixel. A very simple model based on the Thornthwaite's water balance technique is implemented in a daily basis for the period 1999-2014, using daily CHIRPS (rainfall) and 10-day MARS-ECMWF (potential evapotranspiration) data. Although the results are not conclusive, the model has been show promising to include processes that also might trigger the development of an agronomic drought (e.g. distribution of rainfall events and its impact through specific periods of the growing season).

Key words: agronomic drought, Crop Production System Zone, effective rainfall, meteorological drought, NDVI, soil moisture

ACKNOWLEDGEMENTS

First, I would like to express my gratitude to my first supervisor Kees de Bie for his support, constructive criticism and enriching discussions. He guided me to start thinking in a scientific manner, without losing sight on the essential.

I would like to thank my second supervisor Ben Maathuis for his valuable feedback and assistance during my whole research.

My appreciation also goes to Anton Vrieling for his suggestions and comments during the field work in Ethiopia. Extensively, I would like to thank to NMA staff and other organizations visited in the trip for sharing their experiences in relation to drought index insurance projects and possible sources of validation.

My deepest gratitude goes to the course coordinators Raymond Nijmeijer and Petter Pilesjö, who helped me with all the administrative requirements. Special thanks to all the staff and teachers of Lund University and ITC for their advice and support during my studies.

Thanks to my family in Enschede, Emile Mahabub, Phanintra Soonthornharuethai, Noshan Bhattarai and Mirza Cengic for all the encouragement and willingness to help me through all this process.

Thanks to my family and friends for the long distance support. Specially to my father, my mother and my brother, who always have encouraged me to pursue my dreams. Once more, I repeat it to you, *"If I have seen further it is by standing on the shoulders of giants"* (Isaac Newton).

TABLE OF CONTENTS

LIST OF FIGURES

LIST OF TABLES

ABBREVIATIONS

Ac	Soil water holding capacity
APWL	Accumulated potential water loss
CCD	Cold Cloud Duration
CFS	Couple Forecast System
CHIRPS	Climate Hazards Group InfraRed Precipitation with Station data
CHPclim	Climate Hazards Group Precipitation Climatology
CPS	Crop Production System Zone
Dekade	10-days period
Dp	Deep percolation
ECMW	European Centre for Medium-Range Weather Forecasts
Eo	Evaporation
ETo	Potential evapotranspiration
FAO	Food and Agriculture Organization of the United Nations
GHCN	Global Historical Climate Network
GIACIS	Geodata for Innovative Agricultural Credit Insurance Schemes
GSOD	Global Summary of the Day
GTS	Global Telecommunication System gauge
NDVI	Normalized Difference Vegetation Index
Reff	Effective rainfall
SM	Soil moisture
TMPA 3B42 v7	Tropical Rainfall Measuring Mission Multi-satellite Precipitation Analysis version 7

1. INTRODUCTION

1.1. Background

Drought is the most frequent natural hazard in Ethiopia, where at least one event has occurred per decade since 1970 (Gebrehiwot, Van der Veen, & Maathuis, 2011). The national economy is highly threatened by these events as the rain-fed agriculture accounts for approximately 45% of the Gross Domestic Product and provides 73% of employment (Agricultural Transformation Agency, 2014).

To reduce the vulnerability of the agronomic sector to drought, different financial strategies have been implemented, such as the expansion of credit schemes and the development of drought insurance products (Agricultural Transformation Agency, 2014). In detail, indemnities are paid according to anomalies detected in the measurements of rainfall (meteorological-gauges) or satellite information of crop status (Dinku et al., 2009; Stanimirova et al., 2013). Although some of these products have been already offered to the Ethiopian farmers, several technical and institutional issues still remain for their applicability to larger scales (Gommes & Kayitakire, 2013).

Specifically, the most critical aspect in the design of these strategies is related with the selection of the environmental parameters and sources of data used for the assessment of droughts. As a matter of fact, multiple meteorological, agronomical, hydrological and social processes are studied to account for the different spatial and temporal scales of drought events. For instance, rainfall amount and frequencies relate to shortages in plant water availability (Nagarajan, 2010), but the occurrence of drought events also depends on other meteorological parameters (e.g. temperature and wind), hydrometereological processes (e.g. evapotranspiration and runoff) and local conditions (e.g. type of soil and crops).

In this domain, remote sensing is relevant as it can provide measurements which are spatially continuous and with high temporal resolutions (Mishra & Singh, 2011). Indeed, the use of satellite vegetation indices as the Normalized Difference Vegetation Index (NDVI) has proven to be correlated with parameters associated to growth crop status (e.g. biomass accumulation, leaf chlorophyll levels and fractions of absorbed photosynthetically active radiation) (Lillesand, Kiefer, & Chipman, 2014). However, the unique use of these techniques does not allow to define the exact cause of an observed anomaly in the crop status (Chuvieco & Huete, 2010).

In order to establish water stress conditions, the growth status monitored using NDVI has been studied in relation to time-series of different explanatory variables (e.g. rainfall, and soil moisture) (Eklundh, 1998; Gessner et al., 2013; Herrmann, Anyamba, & Tucker, 2005; Hoscilo et al., 2014; Propastin, Kappas, Erasmi, & Muratova, 2007; Tapiador et al., 2012; Udelhoven, Stellmes, del Barrio, & Hill, 2009). The differences among these studies consist mainly of lag relationships identified, the thresholds used to establish the occurrence of a drought event and the techniques implemented to account for statistical issues in the time-series analysis, such as autocorrelation, non-stationarity effects and presence of trends.

Considering the advances of these studies and the general difficulties experienced by some satellite drought insurance projects to identify accurately the areas affected by drought events (Dinku et al., 2009; Osgood, 2010), it is of special interest the exploration of potential validation techniques. Indeed, the relationship between the vegetation indices and effective rainfall could eventually be useful to identify the limitations of the models implemented.

1.2. Problem statement

The amount distribution and intensity of rainfall, is a key weather parameter affecting the Ethiopian agriculture (Degefu, 1987). In fact, deviations from the regular rainfall pattern can easily trigger the development of meteorological drought, defined as the *"deficiency of rainfall compared to normal rainfall in a given region"* (Gebrehiwot et al., 2011). This event can led to agronomic, hydrological and eventually to socioeconomic drought (Nagarajan, 2010).

Considering that an agronomic drought is a physical manifestation of meteorological drought (Boken, 2005), defined as *"periods with declining soil moisture and consequent crop failure*"(Mishra & Singh, 2010), the scientific model supporting the project Geodata for Innovative Agricultural Credit Insurance Schemes (GIACIS) in Ethiopia uses NDVI as a proxy to establish occurrence of agronomic droughts in 24 key Crop Production System Zones (CPS). In detail, the CPS zones were delineated by de Bie (2014) according to an hyper-temporal ISODATA clustering analysis of 10-day NDVI time series covering 1998-2013, which is used in this study to calculate the NDVI negative anomalies by zone covering the years 1999-2014 with respect to the related long term median NDVI profiles (agronomic drought).

Previous projects implementing weather insurance schemes in the country have reported some disagreement between what is detected by rainfall-based indexes and what it is experienced on the ground (basis risk) (Stanimirova et al., 2013). From the scientific perspective, one of the possible reasons is related with the required spatiotemporal detail and accuracy that cannot always be captured by satellite-based rainfall estimates. Rainfall is only one of the factors that determines the amount of water that becomes locally available for crops as soil moisture, which also depends on other factors as water holding capacity, distribution and intensity of rainfall, evaporation, runoff, runon, infiltration rate and deep percolation.

With the purpose to establish with more certitude the areas where an agronomic drought event is experienced, this study explores validation options for the GIACIS model using the known lagged relationship between previous rainfall (meteorological drought) and the crop growth assessed by the NDVI (agronomic drought). Meteorological drought is calculated based on the same logic applied to capture negative NDVI anomalies. Simple adjustments to account for the effective rainfall or "*rainfall useful for meeting crop water requirements*" (Doorenbos & Pruitt, 1977) are also explored considering the losses by deep percolation, evaporation and runoff.

To summarize, this research differs from previous studies consulted in the monthly NDVI-rainfall relationship (Eklundh, 1998; Herrmann et al., 2005; Hoscilo et al., 2014), as the CPS scheme and the translation of rainfall values in effective rainfall allows the development of relationships that might represent in a more realistic way what happens on the ground during a growing season at a dekadal (10-days) temporal resolution. The analysis of this relationships at a CPS level is very innovative, as it covers the need specified in Hutchinson (1991) of studying the overall development of the drought events in agricultural regions that are homogeneous in terms of macro-scale variables, such as: climate, land cover, management practices and soils.

In fact, the use of this stratification removes the macro-scale processes and allows to focus on the local physical factors that explain differences in the development of agronomic droughts based on differences in rainfall (weather).

1.3. Research objectives

1.3.1. General objective

The general objective of this research is to explore options to validate agronomic drought as assessed by NDVI time series through satellite derived estimates of rainfall, with focus over selected Crop Production System Zones (CPS) of Ethiopia and for the years 1999 to 2014. In order to accomplish this, the subsequent objectives are specified;

1.3.2. Specific objectives

1. To establish the averaged long term temporal relationship between median NDVI and rainfall across pixels within each selected CPS-zone during their associated growing seasons.
2. To improve the above relationship for the region of Tigray (CPS-7) to mimic better aspects of effective rainfall through the use of options like (i) capping rainfall (to mimic water losses during periods of excess rainfall) and (ii) setting fixed losses (to mimic daily losses due to evaporation).
3. To explore the agreement of seasonal negative anomalies of NDVI and of rainfall using the above identified relationship at zone level for the region of Tigray (CPS-7).
4. To explore the visual agreement of seasonal NDVI negative anomalies and of modelled soil moisture at a pixel level.

1.4. Research questions and hyphotesis

- Pertaining to specific objective 1: What is the long term optimal lag relationship between NDVI and rainfall in each selected CPS?

  R/ A linear model with a rainfall lag between 1 to 9 dekades (10-day periods).

- Pertaining to specific objective 3: Do the seasonal negative NDVI anomalies correspond spatially with the seasonal negative lagged rainfall anomalies*?

  R/ Seasonal negative NDVI and lagged rainfall anomalies are related with a Kappa coefficient above 75%.

  *Applicable for good and bad years
  *Considering a categorical classification of the anomalies calculated

2. STUDY AREA

2.1. Location

The study area comprises of 24 Crop Production System Zones (CPS) that have substantial cereal areas within Ethiopia as delineated by de Bie (2014) and based on a hyper-temporal ISODATA clustering analysis of 10-day NDVI-images in the period May 1998-December 2013 (SPOT-VGT, 1km²) (See details in Appendix A). The zones are located between latitudes 14° 51' - 3° 23' (North-South) and longitudes 34° 8' - 43° 37' (East-West), and cover a surface of 353.413 km² (Figure 1).

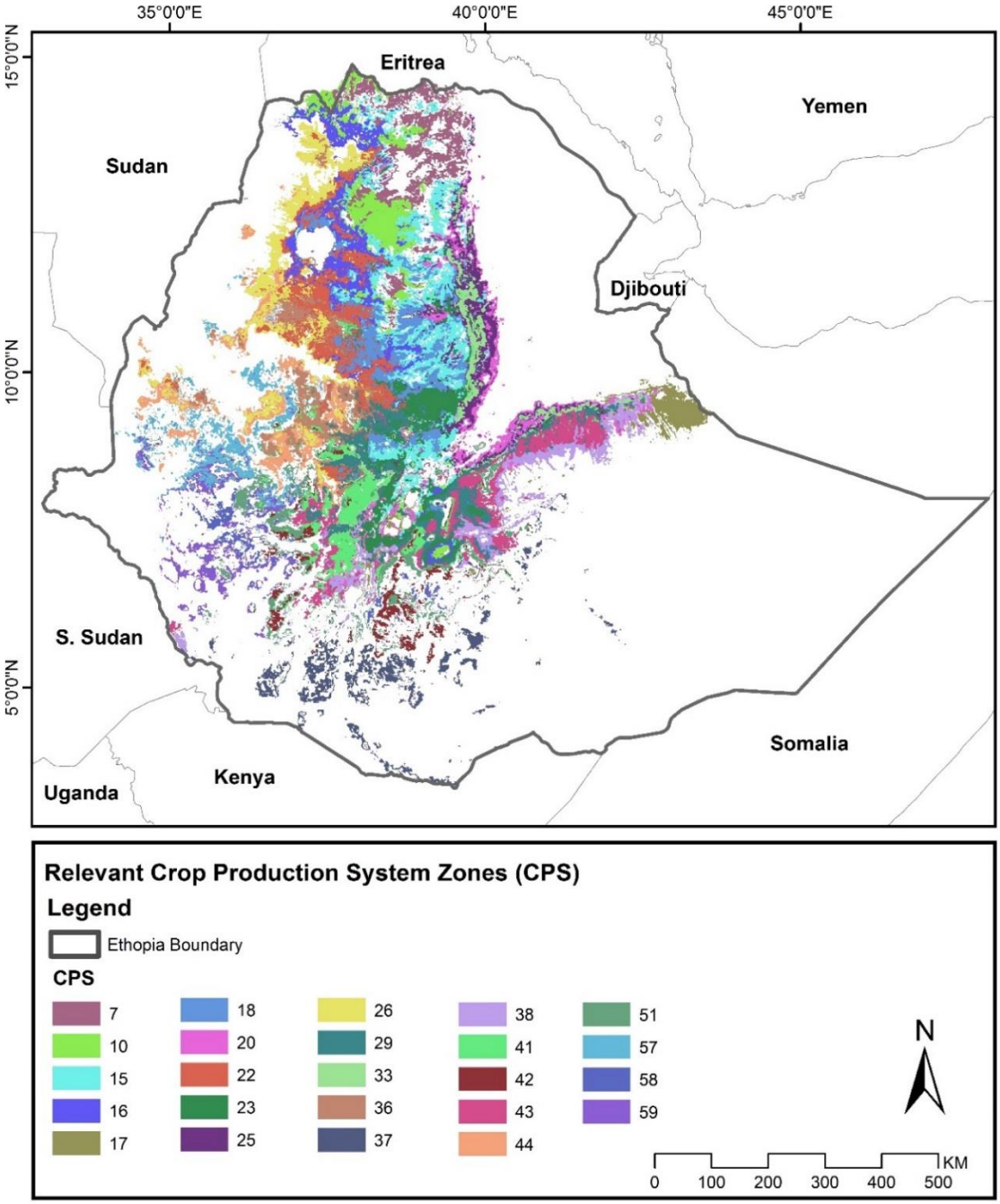

Figure 1. Relevant Crop Production System Zones (CPS) of Ethiopia

The zones are located in the highlands of the country (above 800 m.a.s.l), where the surface occupied by crops is above 5% of the area. Moreover, each CPS is described by de Bie (2014) according to its long term NDVI profile, the associated growing season and percentages of crops cultivated (teff, wheat, barley, beans and maize). The start and end of the growing season for each CPS is derived by de Bie (2014) according to the method explained in Reed et al. (1994). In detail, the start of the growing season is determined as the value where the NDVI profile is crossed by the moving average of the NDVI considering the 9 previous dekades. The same procedure is applied for the end of the growing season, but considering the moving average in reverse.

For the purpose of this study, four zones representing different climatic conditions within the country are selected (Figure 2). The area and percentages of crops associated is presented in Table 1.

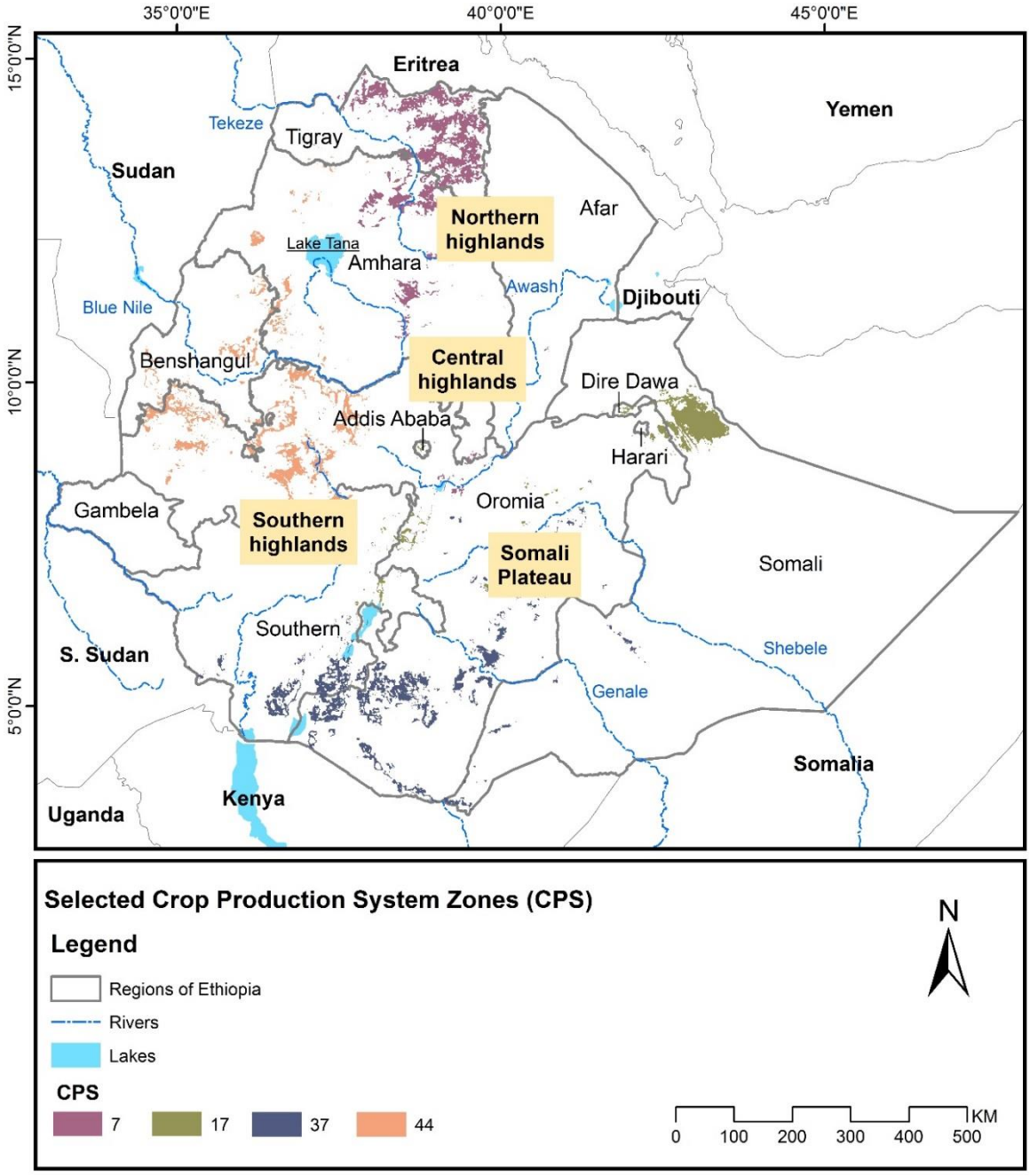

Figure 2. Selected CPS

Table 1. Percentage and type of crops cultivated in each of the selected CPS

	Area (km^2)	Teff (%)	Wheat (%)	Barley (%)	Maize (%)	Sorghum (%)
CPS 7	17722	4	4	3	0	4
CPS 17	8193	0	0	0	3	3
CPS 37	15010	0	0	0	5	5
CPS 44	14358	0	0	0	7	4

*Area given in the projection system Plate Carrée

2.2. Climate

The differences between the amount and distribution of rainfall in Ethiopia are related mostly with the seasonal movements of the Intertropical Convergence Zone (ITCZ), which determines in overall a bimodal rainy season in the south and a unimodal rainy season in the north, (Diro, Toniazzo, & Shaffrey, 2011). Specifically, the related atmospheric circulations come into the country from the southwest and move through the north and back to the south approximately until mid-July and mid-October, indicating the local starting and end of the growing season (Degefu, 1987).

In addition, the sharp topography of the country leads to the occurrence of large orographic effects (Fazzini, Bisci, & Billi, 2015), affecting the local rainfall variability in time and space (Degefu, 1987). Indeed, the study realized by Fazzini et al. (2015) identified a week relationship between precipitation and altitude, which is also characterized by frequent high intensity rains occurring typically in April and August. In spite of these variabilities, the rainfall has an annual average of 800 mm in the country and presents maximum and minimum values respectively in the western highlands and the north-east (geological depressions in Afar region) (Figure 2) (Fazzini et al., 2015). Alternatively, the average annual temperature decreases approximately 6°C every 1000 m, starting by average annual values between 5°C and 10°C in the highest altitudes (3450 and 4300 m.a.sl) (Fazzini et al., 2015).

2.3. Soils and topography

The geomorphological landscapes of Ethiopia are mostly determined by the Great Rift Valley, which crosses the country from southwest to northeast (borders with Kenya and Djibouti) along 900 km, indicating the limit between the north-western highlands (northern, central, southern) and south-eastern highlands (Somali Plateau), which descend smoothly to the lowlands in the Somali region (Figure 2) (Billi, 2015). In overall, the altitudes in the highlands vary between 1500 and 3000 m.a.s.l.

The main lakes of Ethiopia are located along the Rift Valley and the north-western highlands (Lake Tana), where also the general westward slope direct the main rivers (Tekeze, Blue Nile) of the region towards the Nile system in Sudan (Figure 2). Alternatively, the main rivers in the Somali Plateau (Shebele, Genale) flow towards the Indian Ocean crossing the territory of Somalia (Figure 2).

According to the interpretations of Billi (2015) presented in the report realized by UNDP/FAO in 1984, the main characteristics of the geomorphology and soils in Ethiopia are: variable and shallow soils in the northern part of the north-western highlands (CPS 7) and east part of the Somali Plateau (CPS 17), homogeneous and deep soils in the west part of the north-western highlands (CPS 44), and flat landforms and steep slopes with high coverage of Cambisols in the west part of the Somali Plateau (CPS 37). Table 2

summarizes the soil types with highest coverage in each CPS. This information was derived according to the harmonized soil database of FAO (2009) (check map produced in the Appendix B).

Table 2. Main soil types in the selected CPS

CPS 7	Leptosols (58%)	Cambisols (23%)	Other (19%)	Other (0%)
CPS 44	Nitisols (55%)	Leptosols (18%)	Vertisols (12%)	Other (15%)
CPS 17	Vertisols (26%)	Calcisols (20%)	Cambisols (22%)	Other (32%)
CPS 37	Cambisols (31%)	Leptosols (27%)	Luvisols (22%)	Other (20%)

3. METHODOLOGICAL FRAMEWORK

The link between the datasets and methods applied in this study is shown in the Figure 3.

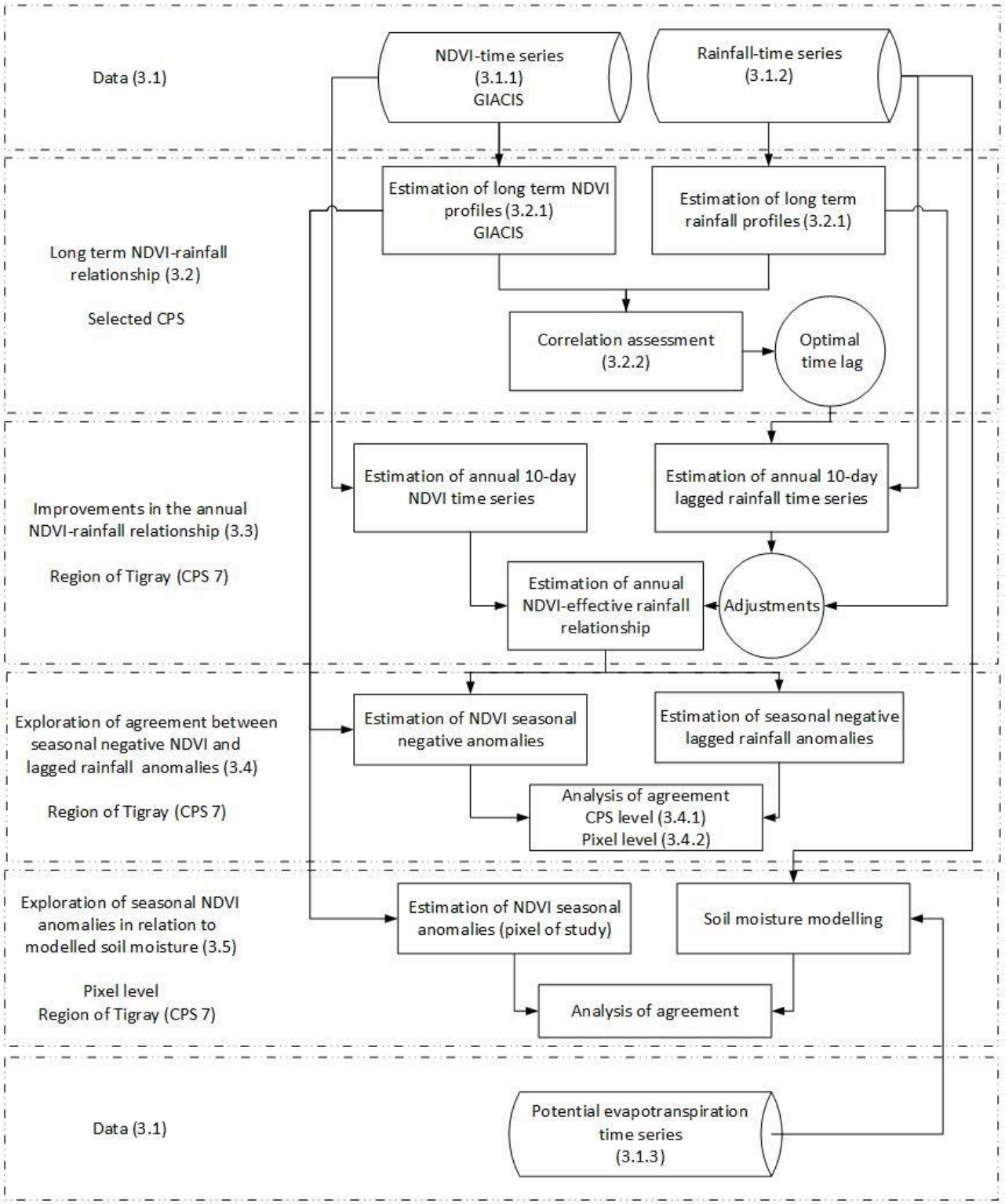

Figure 3. Flowchart of datasets and methods used

3.1. Data

The datasets used in this study consist of the NDVI time series analysis realized by the de Bie (2014), the rainfall satellite product CHIRPS (Climate Hazards Group Infrared Precipitation with Station data) and the potential evapotranspiration from the ERA-INTERIM reanalysis dataset from ECMW (European Centre for Medium-Range Weather Forecasts).

3.1.1. NDVI (SPOT-VGT imagery)

The dataset is composed of 10-day maximum value composite NDVI images by pixel for 1999-2104. In detail, the S10 product (SPOT-VGT imagery) has 1 km spatial resolution and daily global coverage since April 1998 to 2014. In addition to the atmospheric and radiometric corrections associated to the product, the time series have been filtered by de Bie (2014) using the Savitsky-Golay technique to remove residual noise caused by haze and clouds. The NDVI values are represented as digital numbers (DN) according to Equation 1:

$$DN = \frac{NDVI + 0.1}{0.004}$$

Equation 1. NDVI format

Besides the CPS-zone construction explained in the section 2.1, the dataset is composed by the median intra-annual profiles calculated by de Bie (2014) to represent the normal growing patterns for each of the selected CPS (Figure 2). Specifically, the derivation of these profiles consisted of the calculation of the 10-day percentiles (50p and 5p) of all the pixels and for all their 16 annual repeats in one specific CPS (1999-2014).

3.1.2. Rainfall (CHIRPS)

The dataset is composed of 10-day and daily rainfall time-series by pixel for the period 1999-2014. The Climate Hazard Group Infrared Precipitation (CHIRPS) is a global satellite product with 0.05° spatial resolution (5 km approximately) that incorporates in-situ data to produce rainfall estimates since 1981 to present (Dinku, 2014). In detail, the rainfall is originally estimated in a pentad basis (5-days), but also distributed at other time steps according to aggregation and reescalation procedures (monthly, dekadal and daily resolution).

Selection of the product

The selection of CHIRPS is motivated based on the long term validation work as realized by Dinku (2014) using different rainfall infrared products against in-situ measurements in Ethiopia. The CHIRPS data presents better correlation results (0.57 and 0.61 for March-May and December-February, respectively) compared to TAMSAT (Tropical Application of Meteorology using Satellite and other data) and ARC (Africa Rainfall Climatology).

The validation realized by Funk et al. (2015) using Global Precipitation Climatological Centre (GPCC) stations as reference indicates that the CHIRPS data has less bias compared to other satellite products (Tropical Rainfall Measuring Mission Multi-satellite Precipitation Analysis version 7 (TMPA 3B42 v7)), reanalysis models (Coupled Forecast System (CFS) and ECMWF and gauge measurements (CPS Unified interpolated gauge product). For the wettest three months of the years 2000-2010, the CHIRPS exhibits an average bias of 0.22 over Africa (bias=abs(1-mean(satellite)/mean(GPCC)) with a correlation coefficient of 0.56. The other products present higher bias values between 0.3 (CPCU) and 0.43 (CFS), and correlation values between 0.3 and 0.6 (TMPA 3B42 RT7 and CPCU, respectively).

The selection of CHIRPS is also motivated by its low latency (3 weeks), incorporation of rain gauge measurements in the algorithm, the long period of record and the improved spatial resolution in comparison to other products that merge satellite estimates with in-situ data (e.g. The Climate Prediction Center Merged Analysis of Precipitation with a resolution: 2.5°).

Technical specifications

The algorithm consists of three main components, which are: the Climate Hazards Group Precipitation Climatology (CHPclim), the CHIRP and the merging process with meteorological stations (CHIRPS). Based on Funk et al. (2015), the main considerations for the development of each of these components are summarized below:

- Climatology CPHclim

The climatology CHPclim (0.05° spatial resolution) is based on the long-term monthly measurements of 27.453 and 20.591 meteorological stations from the Food and Agriculture Organization of the United Nations (FAO) and the Global Historical Climate Network (GHCN) respectively. In detail, the development of the CHPclim involves the fitting of the FAO measurements to regressions models that consider different physical and satellite covariates (elevation, latitude, longitude, slope, land surface temperature and rainfall estimates from the TMPA 3B42 v7 and the Climate Prediction Center MORPHing Technique (CMORPH)).

Once the regression models are established, the residuals are interpolated and added to each pixel regression model. In addition, the GHCN data is used to correct the bias associated to the station estimation from FAO. Afterwards, the values are interpolated and upscaled to 5-day temporal resolution.

- CHIRP

The main principle behind CHIRP consists of the establishment of a temperature threshold that indicates the presence of a cold cloud and therefore the development of a rainfall event. Considering that the temperature decreases considerably with atmospheric height, the amount of rainfall is estimated according to the time that a high cold cloud is located in a specific pixel (Cold Cloud Duration-CCD) (Tapiador et al., 2012).

In detail, CHIRP uses a fixed threshold of 235°K to establish the presence of cold clouds in the thermal infrared measurements generated by NOAA's National Climate Data Center for the years 1981-2008 (GridSat) and 2000-present (CPS TIR). Afterwards, these CCD values (5-day basis and 0.25° spatial resolution) are calibrated using the rainfall estimates of TMPA 3B42 v7 (with stations). However, if an infrared measurement is missing, the values are set according to the estimates of CFS version 2.

Subsequently, the calibrated CCD values are normalized considering the long term CHIRP precipitation in a 5-day basis (1981-2013) and the associated CHPclim value, which allows to reduce the systematic bias of the satellite estimation. Moreover, these values are resampled to 0.05° spatial resolution and aggregated in longer time steps (10-day and monthly). Likewise, the CHIRP values are downscaled to daily estimates according to the values of the CFS.

❖ CHIRPS

The databases used in the merging process are the GHCN (monthly and daily), the Global Telecommunication System gauge (GTS, daily), the Global Summary of the Day (GSOD, monthly) and the Southern African Science Service Centre for Climate Change and Adaptive Land Management (SASSCAL, monthly). Initially, a selection of meteorological stations is realized prioritizing the national databases (e.g. GSOD) and the presence of only one station within a 5km ratio. In addition, the extreme values in the associated time series are excluded ($>|\ \pm 4\sigma|$) and the zero rainfall values in the daily products (GHCN and GTS) are omitted when the associated daily CHIRP estimate is above normal.

Once the meteorological stations are selected, an inverse distance weighting interpolation of the bias is realized considering the ratio between the in-situ measurements ($s_{1.5}$) and CHIRP values of the five closest stations ($c_{1.5}$) (Equation 2). Subsequently, the CHIRPS values are estimated considering this bias and an adjustment according to the expected correlation between the closest station (R_{ns}) and the in-situ measurements (R_{CHIRP}) (Equation 3).

$$b_{1.5} = (s_{1.5} + \varepsilon)/(c_{1.5} + \varepsilon)$$

Equation 2. CHIRPS blending procedure

$$CHIRPS = \alpha * CHIRP + (1 - \alpha) * b * CHIRP$$
$$\alpha = R_{CHIRP}/(R_{CHIRP} + R_{ns})$$

Equation 3. CHIRPS estimation

3.1.3. Potential evapotranspiration (MARS-ECMWF)

This dataset is compound by the 10-day time series of each pixel potential evapotranspiration (ETo) in the period 1999-2014. Specifically, the data is globally available since 1989 with a spatial resolution of 0.25° (25 km approximately) and a temporal resolution originally daily, which is aggregated and distributed as dekadal values (Maathuis et al., 2014).

The estimates are based on various sources of the EVMWF, including different variables assessed through reanalysis and operational deterministic models (ERA-INTERIM and OPE) (Maathuis et al., 2014). In detail, ETo values are calculated *"according to Penman-Monteith, based on dew point, daily radiation sum, wind speed and temperature"* (Maathuis et al., 2014).

3.2. Long term NDVI-rainfall relationship

3.2.1. Estimation of profiles

The rainfall median intra-annual profiles are generated following the same logic as the NDVI spatial and temporal generalization set by de Bie (2014) to establish the patterns of growth in the selected CPS (section 3.1.1). This method involves the analysis of the rainfall pixels that are totally located inside a specific CPS-area considering their annual 16 repeats (1999-2014) (See Figure 4).

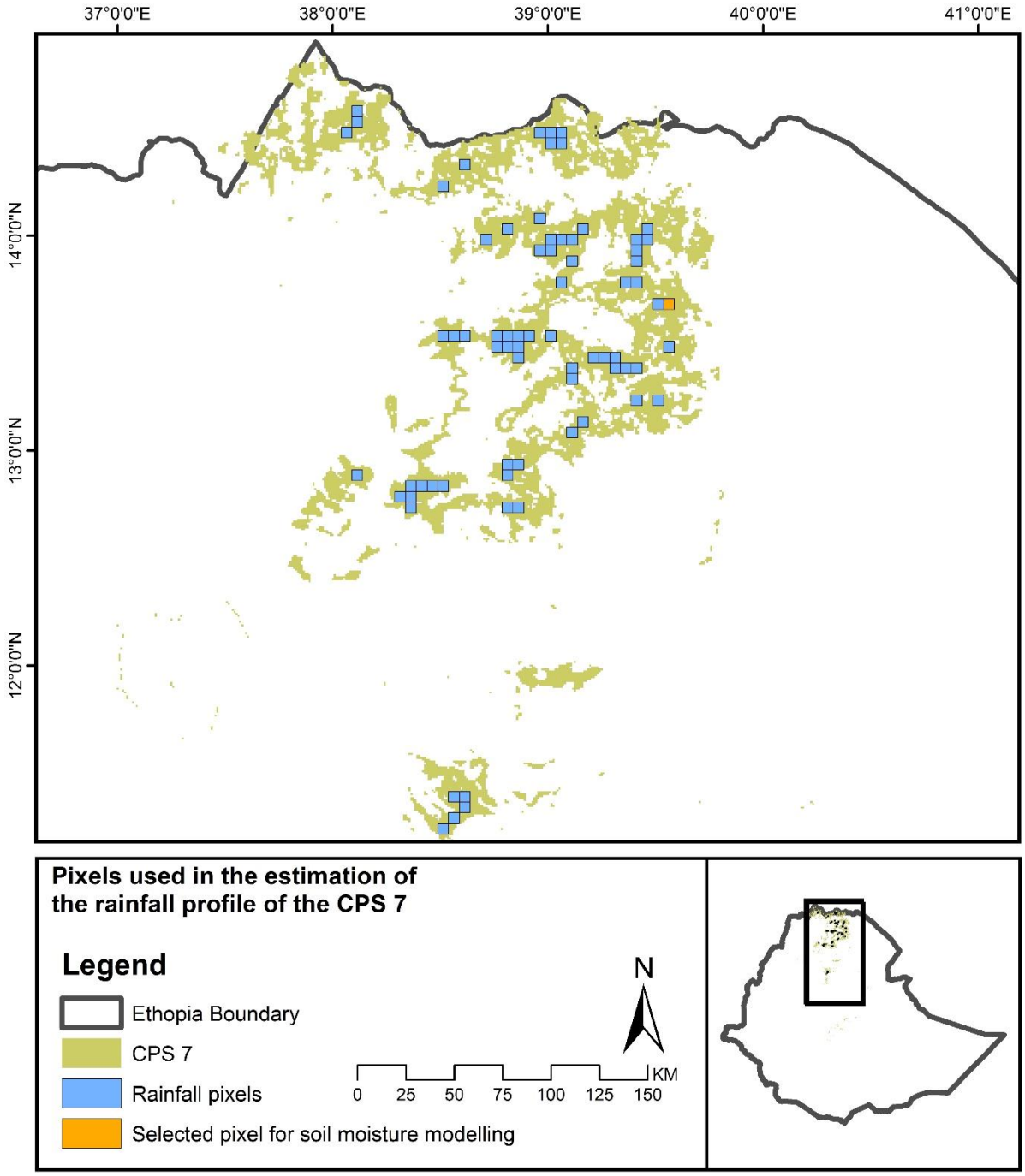

Figure 4. Pixels used in the estimation of the rainfall profiles (CPS 7 - Tigray region)
*Spatial resolution of the pixels: 5 km (CHIRPS)

From all the pixel values, the 50 and 5 dekadal (10-day) percentiles of rainfall are calculated and plotted against the NDVI profiles as described in the section 3.1.1. Subsequently, a visual analysis is performed to describe and compare qualitatively the relationship between the NDVI and rainfall in the different CPS (e.g. profile shapes, correspondence between the NDVI green-up values and maximum 10-day rainfall and relative changes of NDVI and rainfall in the percentiles of analysis).

3.2.2. Correlation assessment

Pearson correlation is performed to evaluate the strength of the linear relationship between the median intra-annual rainfall and NDVI of each selected CPS during their growing season (50 percentile profile calculated in section 3.2).

Considering that previous studies have indicated that NDVI values in a specific period are better related linearly with the average of rainfall up to 3 preceding months (Davenport & Nicholson, 1993; Grist, Nicholson, & Mpolokang, 1997; Nicholson, Farrar, & Lare, 1994; Nicholson & Farrar, 1994), different correlations are assessed testing the moving averages of rainfall up to 9 previous dekades (10-day periods). In detail, the amount of dekades with the higher correlation coefficient for a specific CPS is selected to capture the optimal time lag. Additionally, the concurrent amount of rainfall is not considered for the moving average calculations because it does not necessarily in time lead to any effect on the current NDVI readings.

3.3. Improvements in the annual NDVI-rainfall relationship (Effective rainfall)

According to Grist et al. (1997) and other early studies pertaining to the relationship between NDVI and rainfall, there is a threshold value (UT) above which rainfall stops to be a limiting factor for the development of vegetation and therefore does not contribute to changes in the NDVI (Nicholson & Farrar, 1994; Farrar, Nicholson, & Lare, 1994; Davenport & Nicholson, 1993).

To identify the existence of such a limit for the CPS-7, the linear annual relationship (1999-2014) between the 10-day area-aggregate average of NDVI and rainfall at the optimal lag is calculated and reestablished based on 10-day raw rainfall estimates corrected using fixed thresholds. These modifications account respectively for 10-day losses due to evaporation (Eo) (Equation 4) and deep percolation (Dp) for rainfall surplus above the stated limit (Equation 5). Simultaneously, the rainfall median intra-annual profiles are modified accordingly.

$$R_1 = 0, if\ R \leq 25mm$$
$$R_1 = R - 25, if\ R > 25mm$$

Equation 4. Lower threshold

$$R_2 = R_1, if\ R_1 \leq UT$$
$$R_2 = UT, if\ R_1 > UT$$

Equation 5. Upper threshold

The selection of the lower threshold (Equation 4) resembles the "fixed percentage" empirical method recommended by FAO (Doorenbos & Pruitt, 1977) to estimate effective rainfall, while the upper threshold is set according to the visual analysis of the annual NDVI-rainfall linear relationship.

3.4. Exploration of agreement between seasonal negative NDVI and lagged rainfall anomalies (CPS-7)

3.4.1. CPS level

Anomalies are calculated for the CPS-7 following the threshold level method described by (Van Loon & Van Lanen, 2011) (Equation 6), where X_t is the area-aggregated average of the NDVI at a specific dekade t and X_{LT} the median intra-annual NDVI during identical 10-day period. Likewise, the lagged rainfall anomalies are calculated using the modified values as generated in section 3.3.

$$d = X_t - X_{LT}$$

Equation 6. 10-day anomalies

In order to analyse the agreement between negative NDVI and lagged rainfall anomalies, the 10-day values are compared for each year and the applicable growing season. A simplified approach is also performed considering the annual sum of the negative anomalies (1999-2014).

3.4.2. Pixel level

The spatial agreement of anomalies is explored at a pixel level considering the application of the simplified approach explained in 3.4.1 (where X_t is replaced by the pixel-aggregated average of the NDVI at a specific dekade t) and the use of the confusion matrix and Kappa coefficient. At a pixel level, seasonal negative NDVI anomalies of all years of study (1999-2014) are ranked and classified in 4 groups (very bad, bad, good or very good), containing each 4 years. The same procedure is applied for the seasonal negative lagged rainfall anomalies.

The confusion matrix and Kappa coefficient is calculated for a subsample of years that show satisfactory agreement at the CPS level (section 3.4.1), including good and bad years in terms of both NDVI and lagged rainfall anomalies.

In detail, the Kappa coefficient (Equation 7) involves the calculation of the chance of random agreement (CA) and the observed accuracy (OA) or percentage of observations that match in the same category in both datasets (Lillesand et al., 2014). From the confusion matrix, A: number of observations in both datasets matching in the same category, B: number of observations in the NDVI dataset in a specific category, C: number of observations in the lagged rainfall dataset in a specific category and N: number of observations.

$$K = \frac{OA - CA}{1 - CA} = \frac{\frac{\sum A}{N} - \sum B * C}{1 - \sum B * C}$$

Equation 7. Kappa coefficient

3.5. Exploration of seasonal NDVI anomalies in relation to modelled soil moisture at a pixel level

Soil moisture is estimated for a selected pixel (see Figure 4) using Thornthwaite's water balance technique (1955) and the calculation of effective rainfall as recommended by Doorenbos & Pruitt (1977). The model is implemented on a daily basis for the period 1999-2014 and concerns the next steps (Figure 5):

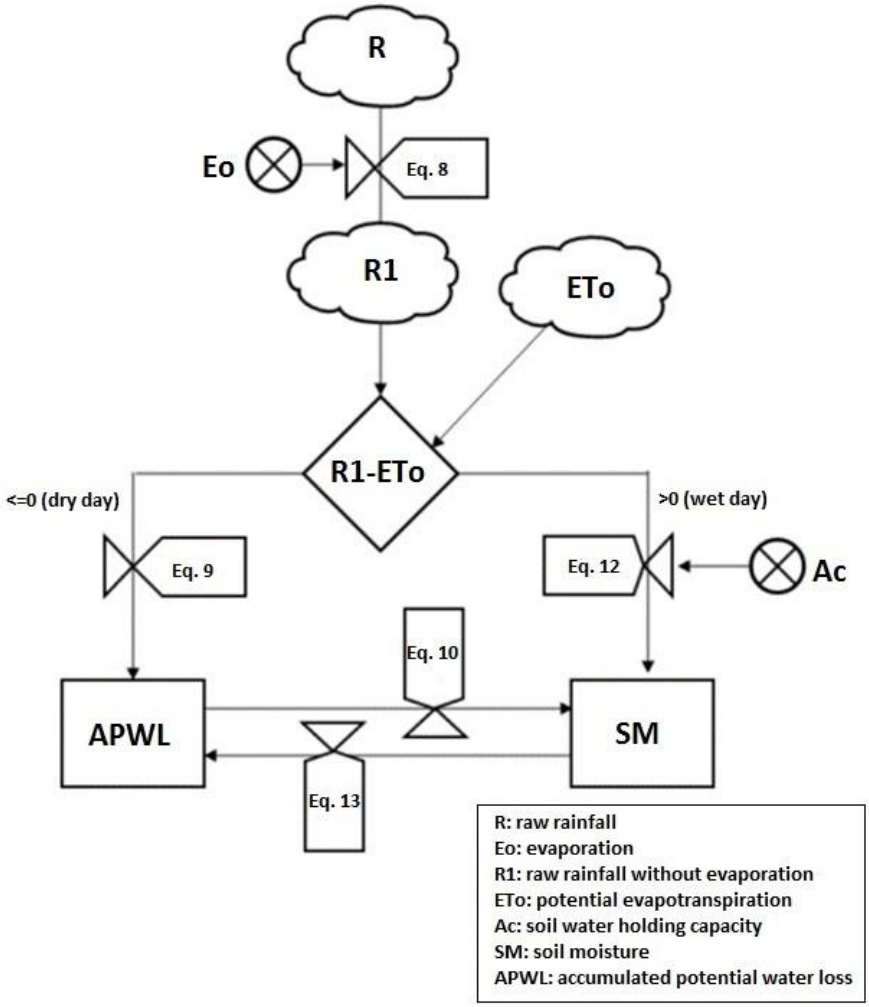

Figure 5. Method for modelling soil moisture

- Rainfall without Eo (R_1)

Considering that all rainfall (R) does not become available for the plants due to Eo (Doorenbos & Pruitt, 1977), the effect of this process is taken into account using Equation 8, where 5 mm is set as the initial threshold .

$$R_1 = 0, if\ R \leq 5mm$$
$$R_1 = R - 5, if\ R > 5mm$$

Equation 8. Rainfall without evaporation

- Soil moisture estimation

The estimation of this variable requires an initial calculation of the difference between the R_1 and ETo. If this balance is negative or equal to 0, the day is defined as dry and the soil moisture balance depletes according to an exponential relationship (Equation 10) which takes into consideration the soil water holding capacity (A_C) and the accumulated potential water loss in the associated day ($APWL_i$) (Equation 9).

$$APWL_i = APWL_{i-1} - (R_1 - ETo)$$

Equation 9. Accumulated potential water loss in a dry day

$$SM_i = A_C * e^{(\frac{APWL_i}{A_c})}$$

Equation 10. Soil moisture balance in a dry day

In the Equation 11, A_C represents the relationship between the effective root depth in mm (Z_e) and the difference between the soil field capacity (θ_f) and wilting point (θ_w) (Dourado-Neto, Jong van Lier, Metselaar, Reichardt, & Nielsen, 2010). As there is no information available about the soils, this value is set according to the Dp threshold identified in 3.3.

$$A_c = (\theta_f - \theta_w) * Z_e$$

Equation 11. Soil water holding capacity

Furthermore, when the balance between R_1 and ETo is positive, the day is considered as wet and the soil moisture balance is replenish according to the excess of R_1 once the energetic requirements or potential evapotranspiration (ETo) is fulfilled (Equation 12). This replenish amount can never exceed A_C, as all the water above this point is considered Dp. In detail, the $APWL_i$ decrease according to a logarithmic function (Equation 13).

$$SM_i = SM_{i-1} + (R_1 - ETo), if\ SM_i < A_c$$
$$SM_i = A_c, if\ SM_i \geq A_c$$

Equation 12. Soil moisture balance in a wet day

$$APWL_i = A_c * \ln\frac{SM_i}{A_c}$$

Equation 13. Accumulated potential water loss in a wet day

Note: the daily ETo used in this model is rescaled considering the ratio between the applicable dekadal value (Section 3.1.3) and the number of associated days[1].

Finally, the soil moisture (SM) estimates are visually compared with the area-aggregated average of the NDVI anomalies at the pixel of study.

3.6. Software

GEONETCast toolbox (ILWIS) for the retrieval of satellite products. ARCGIS for the pre-processing and editing of results. Scripts in ILWIS and R Studio for the time series analysis and model implementation.

[1] The first and second dekade of each month comprehend the first and second 10 days, respectively. The number of days in the third dekade vary according to the month. For practical purposes, the 29th of February is excluded from the calculations.

4. RESULTS

4.1. Long term NDVI-rainfall relationship

4.1.1. Profiles

The Figure 6 and Figure 7 illustrate the relation between the phenology of vegetation as assessed by NDVI and the long term rainfall for each CPS in a 10-day basis. The figures allow to establish differences and similarities concerning amounts and the occurrence of one or two short/long seasons.

For the CPS 44, a high NDVI value of 211 occurs. It has a median intra-annual rainfall amount of 1409 mm, which exceeds rainfall in the other zones (CPS 7: 641 mm, CPS 17: 400 mm, CPS 37: 583 mm). In contrast, CPS 37 presents the second highest NDVI green up values (1st period: 157, 2nd period: 158). The results further indicate that NDVI responses must be analyzed not only considering rainfall amounts, but also rainfall seasonality, timing and duration.

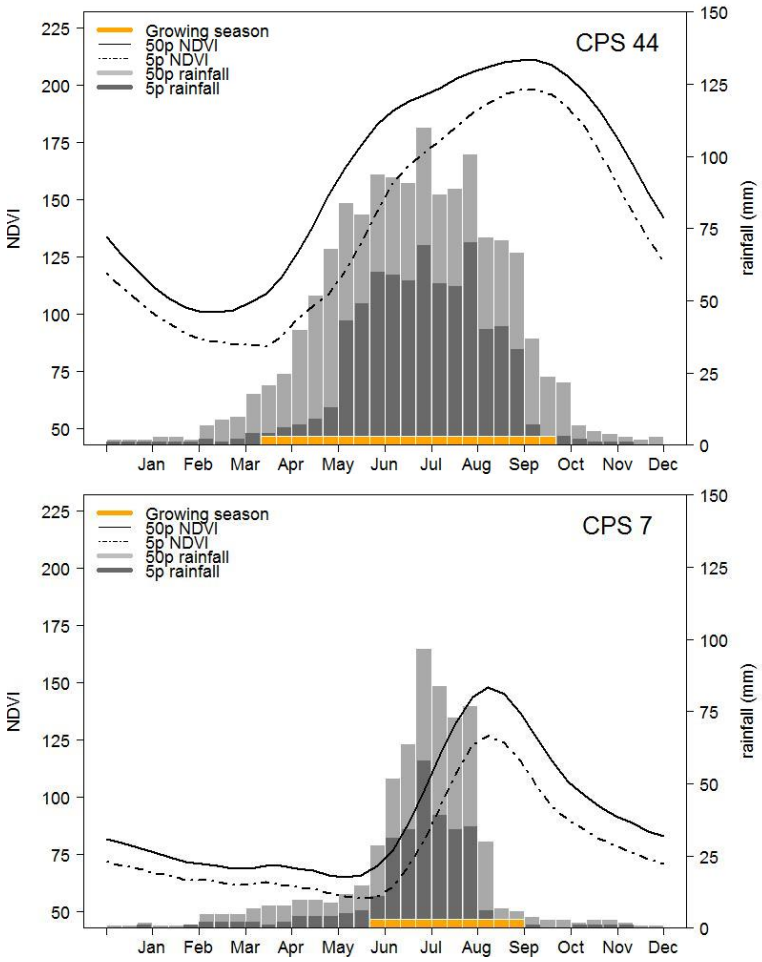

Figure 6. Long term profiles of NDVI and rainfall (CPS with unimodal growing season)

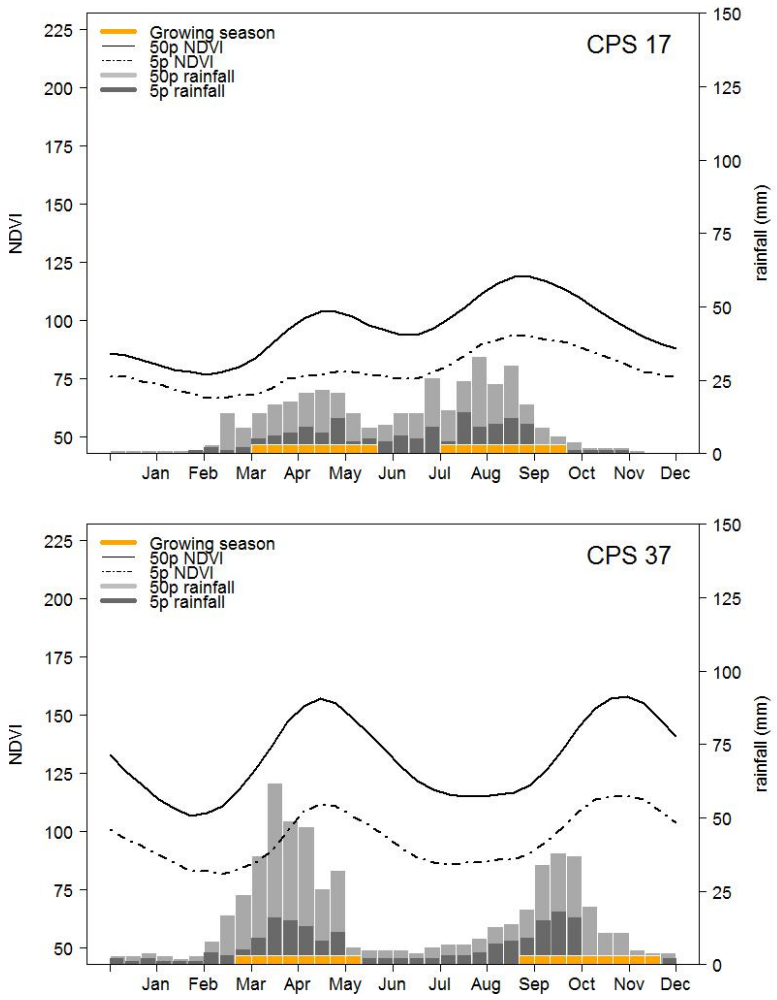

Figure 7. Long term profiles of NDVI and rainfall (CPS with bimodal growing season)

Following this approach, it stands out that the NDVI profile for CPS 44 stays nearly constant at the end of the growing season regardless prior variability in rainfall amounts, while CPS 7 presents a nice bell-shaped NDVI pattern that depicts clearly the rainfall distribution during the growing season (Figure 6). The differences in time between the NDVI and rainfall peaks are approximatelly 4 and 6 dekades (CPS 7 and 44, respectively). This corresponds with the amount of dekades between the greening up of the NDVI and the maximum 10-day rainfall in the median profiles. Likewise, the NDVI profiles with bimodal growing season reflect in general a lag NDVI response to prior rainfall.

The relative annual differences between the 50 and 5 percentile lines for rainfall and NDVI (Figure 6 and Figure 7), are substantially larger for rainfall than for NDVI (Table 3).

Table 3. Annual differences between the 50 and 5 percentile lines for NDVI and rainfall

	Average relative change of rainfall	**Average relative change of NDVI**
CPS 7	59%	18%
CPS 44	55%	16%
CPS 17-1st	59%	23%
CPS 17- 2nd	64%	21%
CPS 37- 1st	69%	30%
CPS 37-2nd	66%	26%

4.1.2. **Correlation**

Table 4 summarizes the Pearson correlations of the median intra-annual profiles of NDVI and different rainfall moving averages for each CPS and its associated growing season (Section 4.1.1). The highlighted values correspond to correlations statistically significant at an alpha level of 0.05.

In overall, the correlations obtained for the optimal time lags (see bold values) vary very little in comparison to the closest lag periods. For instance, the optimal correlation coefficient of the CPS 7 (Lag 6: 0.994) exceeds only in 0.01 the values associated to rainfall moving averages of 5 and 7 dekades, respectively. Already, high correlation values (above 0.75) occurs using short lags for the CPS 17 and CPS 44 (Lag 2 and Lag 1, respectively). CPS 7 and CPS 37 present such correlation values at longer lags (Lag 3 and Lag 4, respectively).

Table 4. Correlation analysis between NDVI and different rainfall moving averages

	Lag 0	**Lag 1**	**Lag 2**	**Lag 3**	**Lag 4**	**Lag 5**	**Lag 6**	**Lag 7**	**Lag 8**	**Lag 9**
CPS 7	-0.189	0.355	0.628	0.842	0.938	0.984	**0.994**	0.986	0.977	0.972
CPS 44	0.514	0.759	0.863	0.911	0.938	0.958	0.964	**0.965**	0.963	0.957
CPS 17	0.242	0.561	0.781	0.917	0.927	**0.933**	0.918	0.903	0.889	0.877
CPS 37	-0.265	0.223	0.453	0.636	0.760	0.820	0.845	0.852	**0.855**	NA

Figure 8 to 11 illustrate the temporal agreement and scatterplot of the median intra-annual NDVI profiles vs. the rainfall at the lag 0 and the rainfall considering the optimal moving average for each CPS. The scatterplots for the CPS 7, 17 and 37 ratify in overall the appearance of a linear tendency that follows the developing of the growing season (see lines connecting the points), while the scatterplot for the CPS 44 displays some trace of a s-shaped relationship.

For CPS 7, the moving average data succeed to smooth out short term variabilities in rainfall, resulting in a temporal agreement between the NDVI green up value and maximum 10-day lag rainfall (Figure 8). Alternatively for the CPS 44, the lag rainfall depicts a slight plateau in the end of the growing season, which resembles to the correspondent NDVI profile (Figure 9). In the related scatterplot, the distribution of the points at the end of the last dekades are poorly associated with variations in rainfall.

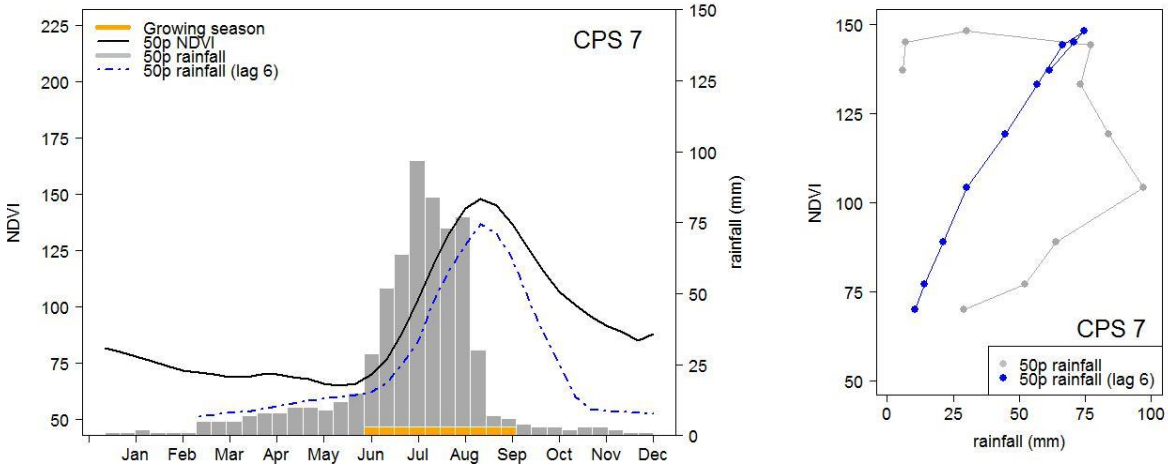

Figure 8. Long term profile of NDVI and optimal rainfall moving average (CPS 7)

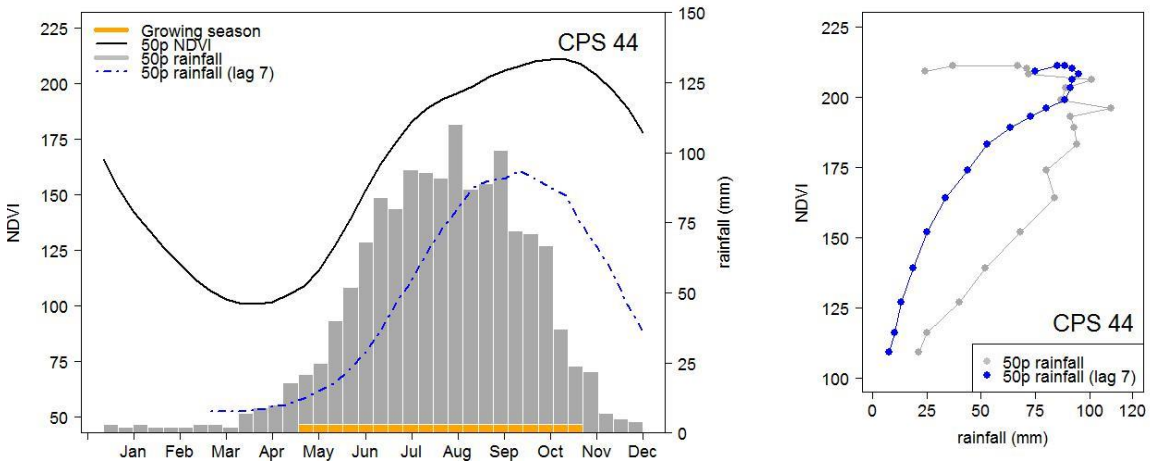

Figure 9. Long term profile of NDVI and optimal rainfall moving average (CPS 44)

The lag rainfall patterns of CPS 17 and CPS 37 follow the correspondent NDVI profiles still, but appear a little out of synchronization by 1 to 2 dekades (Figure 10 and Figure 11). The related scatterplots confirm a linear relationship between the two variables during the beginning of the growing seasons, with some problems relating the two when NDVI peaks and decays.

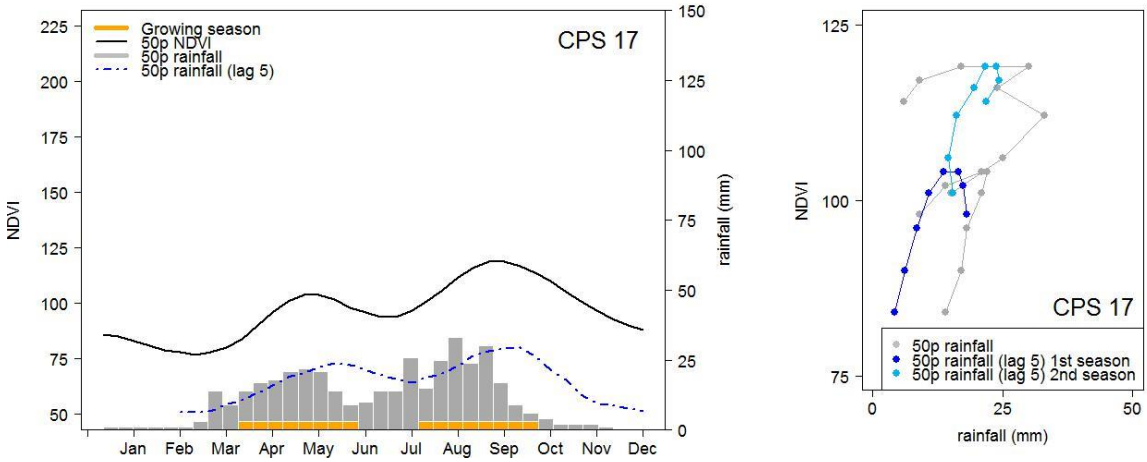

Figure 10. Profile of NDVI and optimal rainfall moving average (CPS 17)

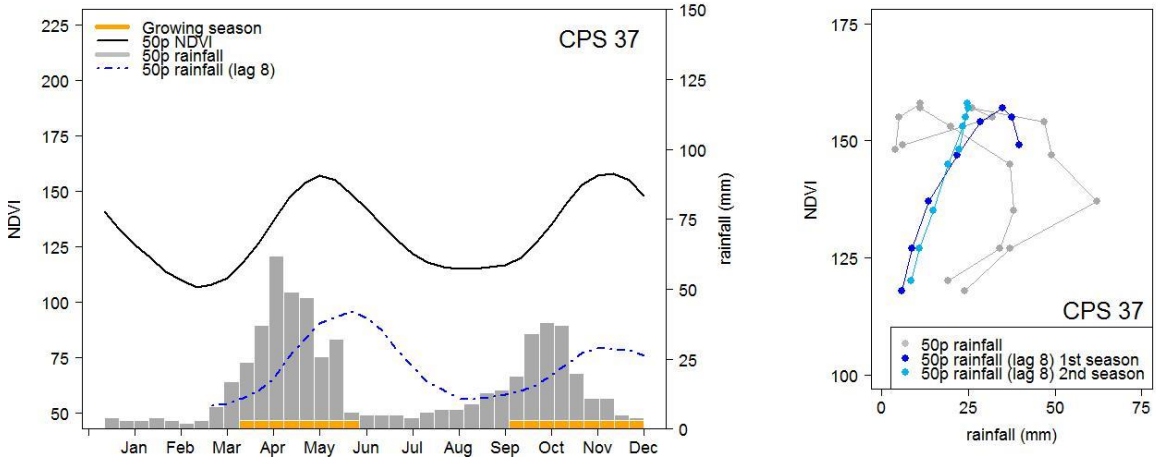

Figure 11. Profile of NDVI and optimal rainfall moving average (CPS 37)

4.2. Annual effective rainfall (CPS-7)

Figure 12 illustrates how the values of the annual NDVI-rainfall relationship during the growing season follow the median intra-annual values as identified in section 4.1.2 (Figure 8), both are based on a moving average of six dekades. The annual NDVI-rainfall relationship between 60-80 mm as occurs during the last dekades of the growing season, appears in the figure as a data-cloud, indicating during that period a slightly increase of the 95% confidence interval.

NDVI estimates derived from recent rainfall records is thus particularly suited for predicting the onset of a season and the period till NDVI peaks, but not for the period afterwards. Other unidentified factors likely take place influencing NDVI development during those later stages, indicating that rainfall loses at those periods is relevant to monitor crop development.

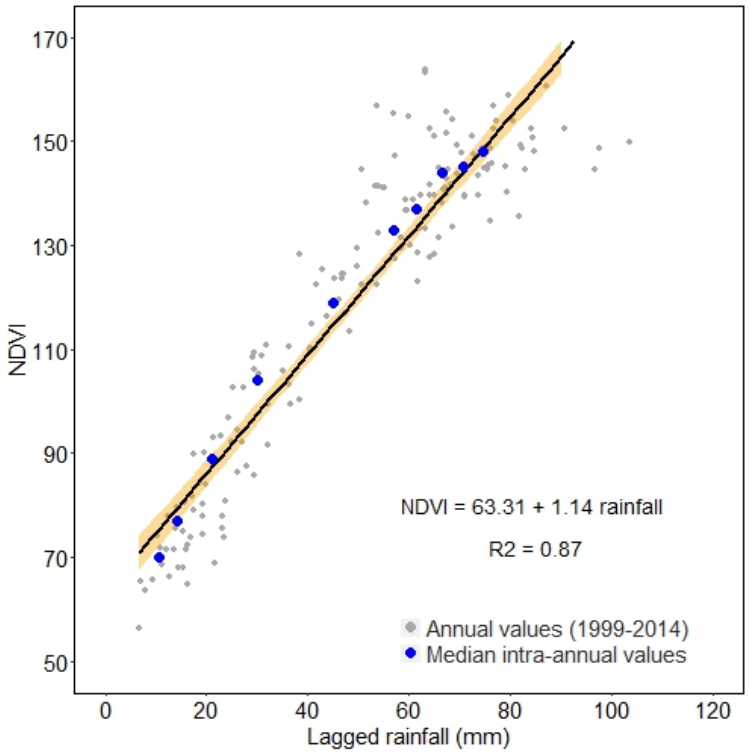

Figure 12. Annual NDVI-rainfall relationship for CPS 7

Using a fixed loss of 25 mm of the original rainfall to account for Eo losses (Figure 13, top) modifies the late season response of the NDVI to rainfall amounts to 40-80 mm. In addition, using a rainfall capping at 50 mm to account for Dp losses (Figure 13, bottom), reduces the scattering of the annual values in the later dekades of the growing season. Both modifications, however still show problems on the predictive power of rainfall at the last dekades. The figures also reflect that all rainfall in the first two dekades of the growing season is lost by Eo.

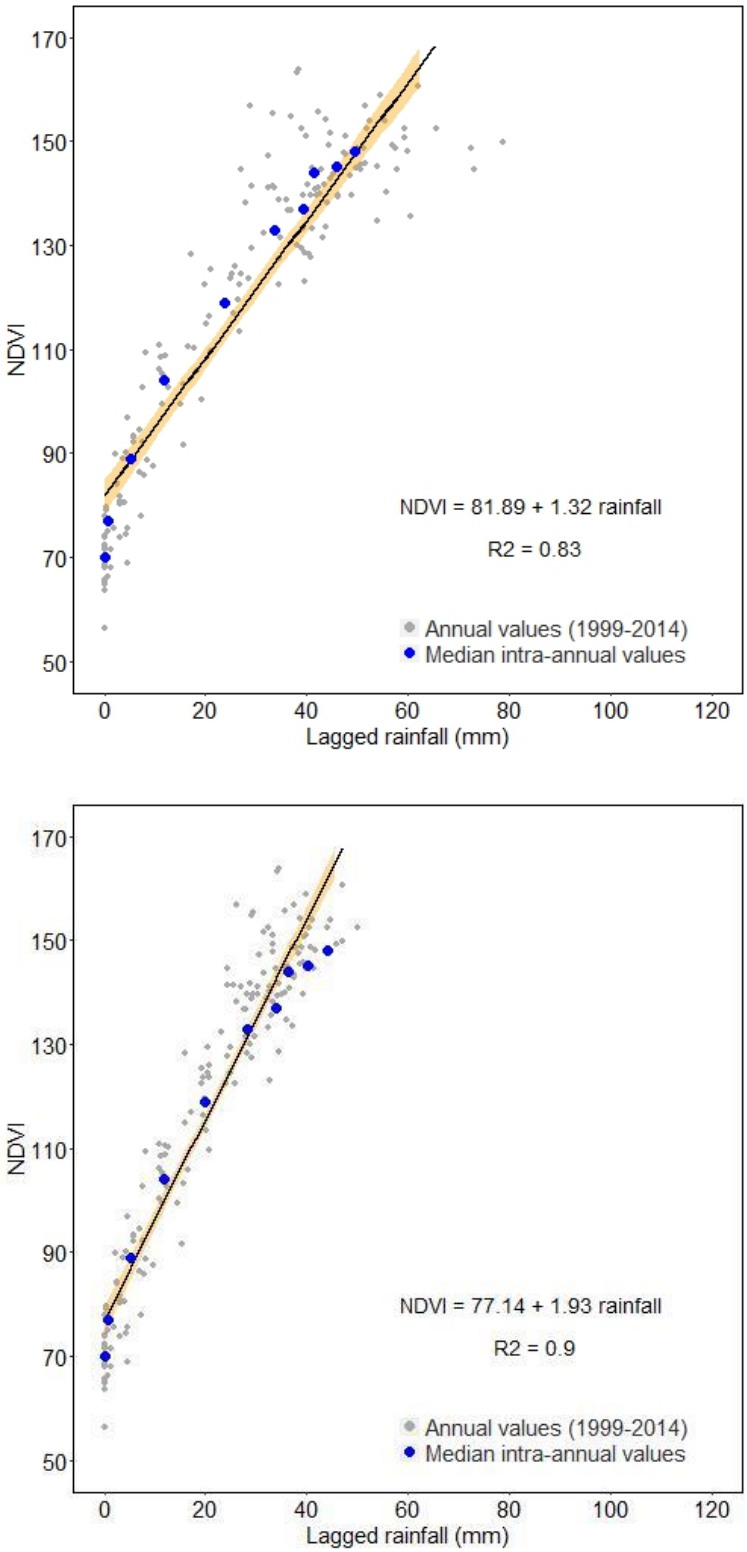

Figure 13. Annual NDVI-effective rainfall relationship for CPS 7
Top (considering set fixed loss Eo), Bottom (considering set fixed loss and capped rainfall, Eo and Dp)

4.3. Agreement between seasonal negative NDVI and lagged rainfall anomalies (CPS 7)

4.3.1. CPS level

Figure 14 summarizes for the area-aggregate data of the CPS 7 (region of Tigray), the relation between the seasonal negative anomalies of NDVI and lagged effective rainfall during the years 1999-2014. The scatterplot suggests a general linear relationship excluding the outlier years in red (3 out of 16 years). For 2008 relatively high seasonal negative NDVI anomalies correspond with low seasonal negative lagged rainfall anomalies, while the opposite situation occurs in 2013 and 2014. This fact already indicates that meteorological drought cannot easily be translated into agronomic drought.

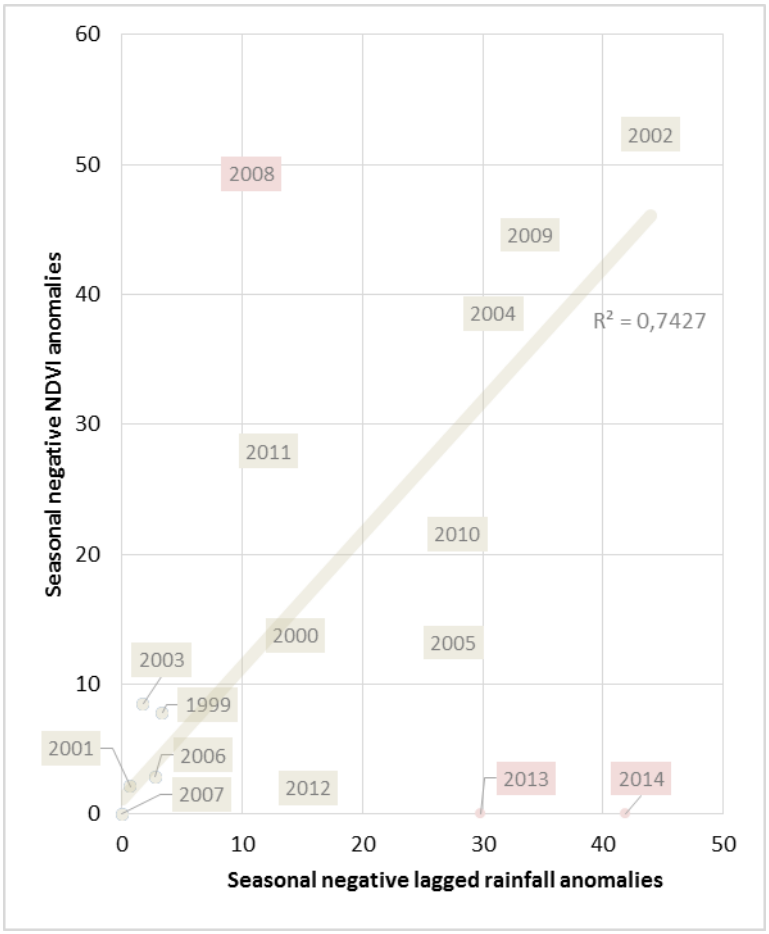

Figure 14. Seasonal NDVI and lagged rainfall negative anomalies for the CPS 7 (1999-2014)

Further details on how these anomalies developed during the applicable growing season can be visualized in Figure 15. For the year 2008, the disagreement between anomalies can be related with a poor distribution of rainfall at the beginning of the growing season, which is not evident considering the analysis of 10-day rainfall amounts. The likely occurrence of spatially extended short duration meteorological droughts (dry spells) at the beginning of the growing season might explain the NDVI negative anomalies at this period.

For the years 2013 and 2014, the disagreement occurs mostly at the end of the growing season, which has already been identified in Section 4.2 as the period with major variability. These dissimilarities can be associated with the little effect that negative anomalies of rainfall have in the last dekades, because of the effect of other macro-scale factors that become more important for crop development (e.g. temperature, solar radiation). The same disagreements observed for the years 2009, 2010, 2011 and 2012 in the last

dekades, can be explained accordingly. Another possibility that explains these disagreements is the need of additional refinement in the estimation of effective rainfall.

For the years 2002 and 2004, shown in the seasonal scatterplot as some of the driest years (Figure 14), the agreement of NDVI and rainfall negative anomalies is consistent through all the growing season (Figure 15). The agreement for the year 2002 is related with the development of a spatially extended drought as shown in Figure 16 (right). For the remaining years (Figure 15), the development of anomalies in both datasets shows an overall positive (1999, 2001, 2003, 2006, 2007) or negative agreement at the end of the growing season (2000, 2005).

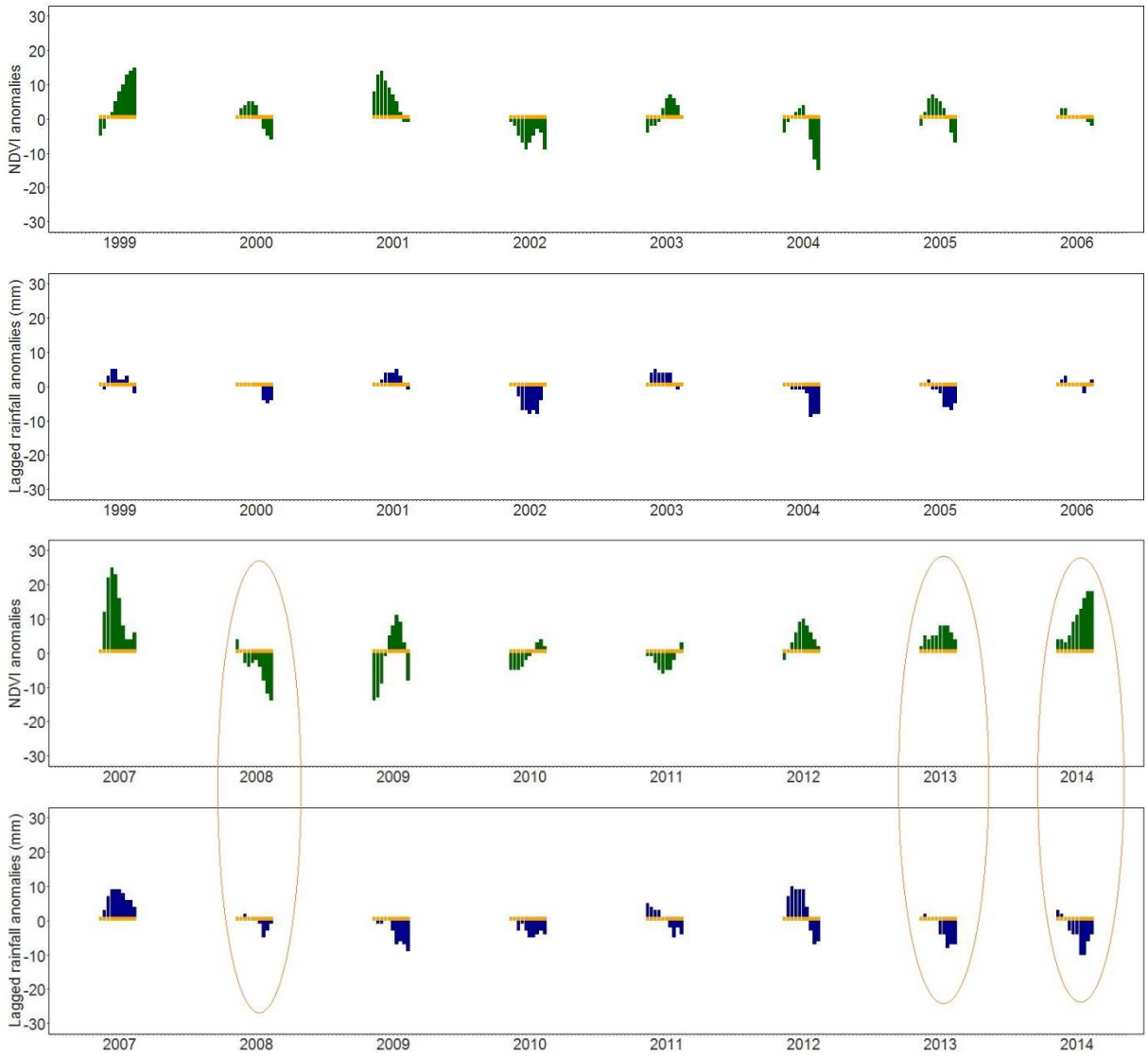

Figure 15. NDVI and rainfall 10-day anomalies for the CPS 7 (1999-2014)

4.3.2. Pixel level

Figure 16 shows the overall spatial agreement of the seasonal negative anomalies for the years 1999 and 2002, using categorical classifications as explained in the section 3.4.2 (see remaining figures in the Appendix C). In detail, the selection of this years is based on the results of the Figure 14, where these years are identified to have a good agreement in terms of both seasonal negative NDVI and rainfall anomalies for the entire CPS.

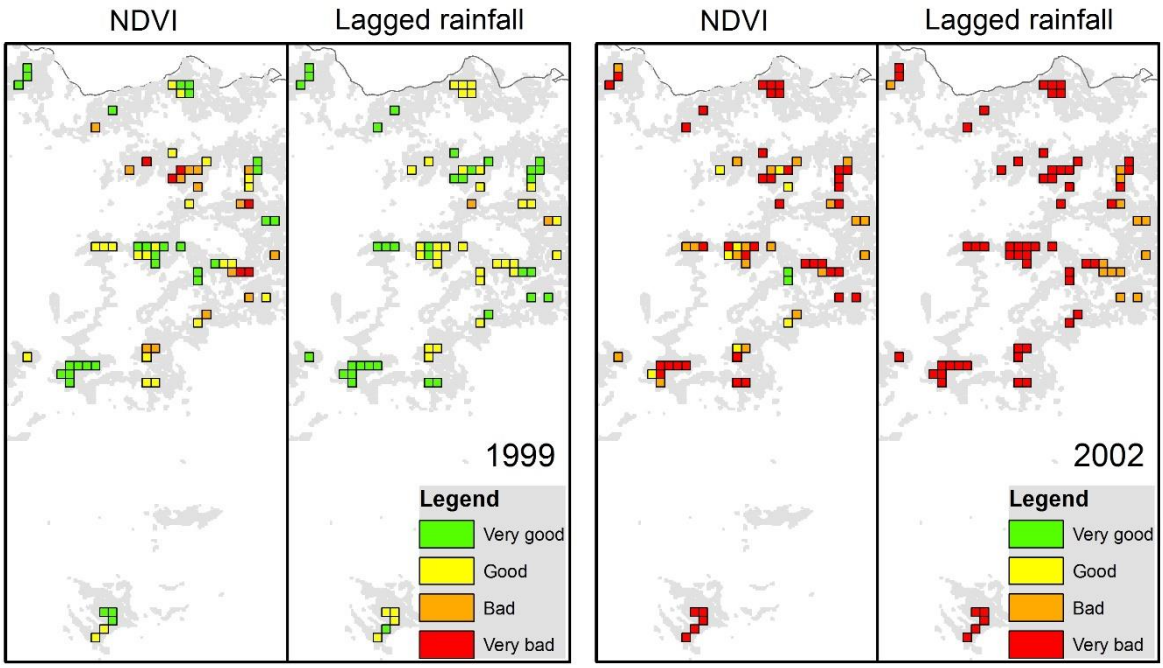

Figure 16. Spatial agreement of seasonal negative NDVI and lagged rainfall anomalies (1999 & 2002)

The related confusion matrix for both years is shown in Table 5. In detail, the percentage of observations matching in the same category for seasonal negative NDVI and lagged rainfall anomalies is calculated as 42.5%, while the chances of obtaining an agreement by chance are estimated in 26.7%. Both measurements confirm that the agreement between anomalies in both datasets is 21.5% better than chance (Kappa coefficient). Therefore, the spatial disaggregation of the years with a good agreement for the entire CPS reduces the predictive power of the relationship (Figure 14), indicating that this level of study still cannot be used in the practice.

Table 5. Confusion matrix between categories of seasonal negative NDVI and lagged rainfall anomalies

	Seasonal negative NDVI anomalies					
Seasonal negative lagged rainfall anomalies	**Class**	Very good	Good	Bad	Very bad	**Total**
	Very good	14	12	6	3	**35**
	Good	15	10	8	3	**36**
	Bad	1	1	4	9	**15**
	Very bad	2	8	16	34	**60**
	Total	**32**	**31**	**34**	**49**	**146**

*Derived according to the years 1999, 2002

4.4. Seasonal NDVI anomalies in relation to modelled soil moisture at a pixel level

Figure 17 (from the top to the bottom) shows for the pixel selected in Figure 5: the NDVI anomalies, the related daily rainfall and potential evapotranspiration values, and the resulting soil moisture estimates during the years 2007-2010 (see remaining years in the Appendix D). In detail, the rainfall estimates consider a set loss of 5 mm to mimic evaporation, while the soil water holding capacity is fixed in 50 mm according to the upper threshold identified in the annual NDVI-rainfall relationship of the CPS 7 (section 4.2).

In overall, the NDVI anomalies at the beginning of the growing season suggests to have a strong agreement with recent rainfall. For the year 2007, the positive NDVI anomalies in the start of the season coincide with the highest amount of rainfall during this period (153 mm), while the early negative anomalies in the year 2010 might be related with poor distribution of rainfall (likely development of a dry spell, * in the Figure 17). Alternatively, the anomalies in the start of the growing season of the years 2008 and 2009 coincide with an insufficient amount of rainfall during this period (68 and 32 mm respectively).

For the year 2010, a well distributed amount of rainfall in the middle of the season (218 mm) is followed by a slowly recover of the NDVI anomalies. For the same period in the year 2007, there are two gaps of more than 10 days without any rainfall that lead to decreases of the soil moisture until approximately 20 mm of depth (+ in the Figure 17), but do not coincide with an abrupt change in the NDVI anomalies (still positive). Considering that the rainfall in the end of the growing season does not surpass 20 mm for any of the years, it can be suggested that the NDVI anomalies in the last dekades depend on previous amounts of rainfall accumulated as soil moisture or other unaccounted effects.

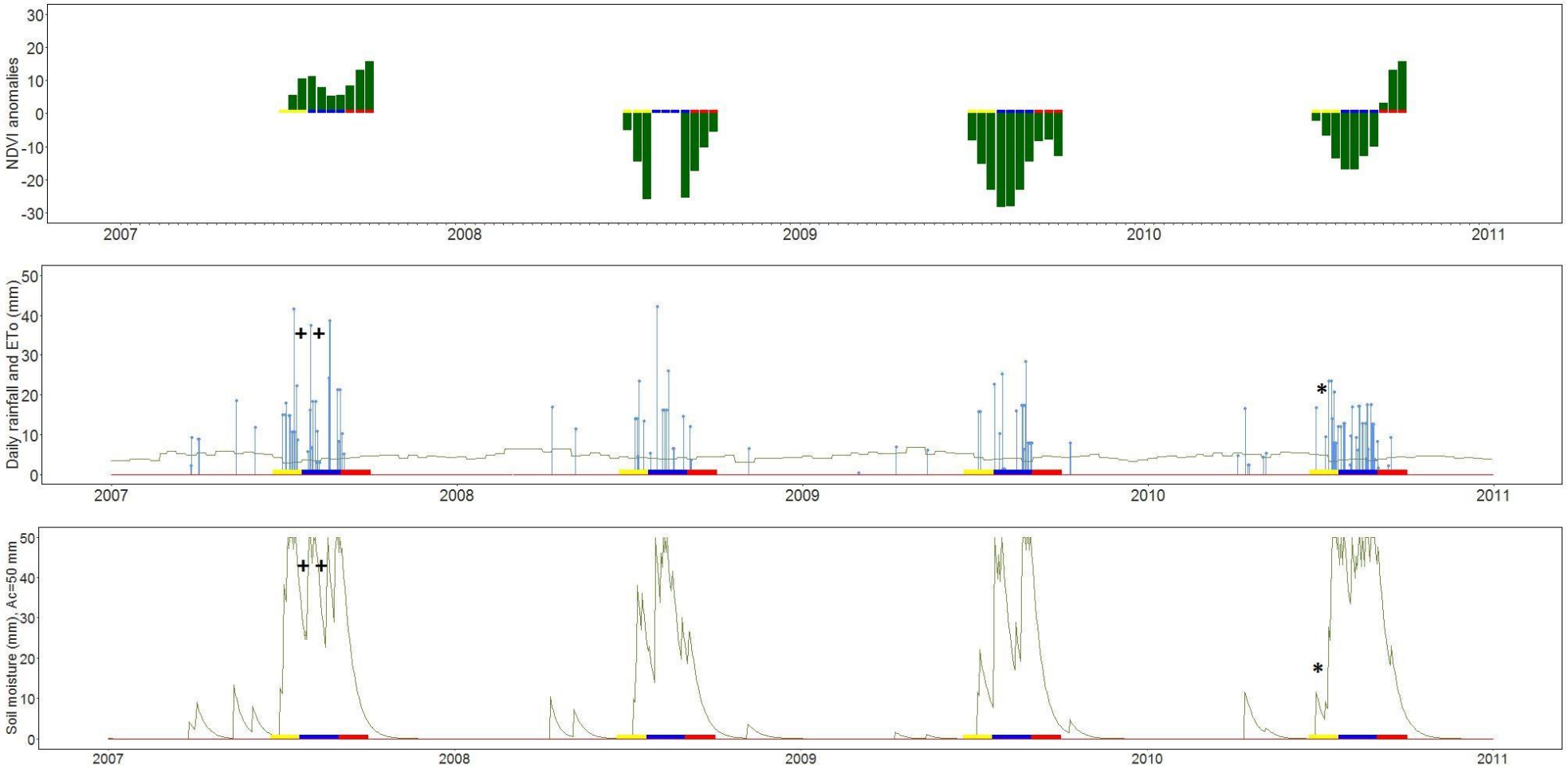

Figure 17. Soil moisture estimates within selected pixel in the CPS 7 (2007-2010)
The growing season appears divided in three segments, which corresponds to: beginning (yellow, 31 days), middle (blue, 41 days), end (red, 31 days)

5. DISCUSSION

5.1. Long term NDVI-rainfall relationship

In the present study, median intra-annual rainfall profiles (10-day CHIRPS data, 1999-2014) for each selected Crop Production System Zone (CPS) are derived to determine their relationship with the median intra-annual NDVI profiles obtained by de Bie (2014). The optimal lag between NDVI and rainfall is identified using Pearson correlation and moving average of rainfall up to 9 previous dekades (10-day periods). Davenport & Nicholson (1993), Grist et al. (1997) and Nicholson & Farrar (1994) have also revealed the effectiveness of this method to analyse the NDVI-rainfall relationship according to specific vegetation covers and soil types.

The NDVI-rainfall profiles and the associated optimal dekadal lags (CPS 7: 6, CPS 44: 7, CPS 17: 5, CPS 37: 8) portrays the general variability that exist among the selected CPS due to differences in macro-scale factors determining the availability of water (e.g. climate, land cover, management practices and soils). These differences as visualized in section 4.1.1 show clear association with the predominant soil types (Table 2). Nicholson & Farrar (1994) related this differences with the soil moisture retention (water holding capacity), which is a parameter that depends mostly on soil texture (Saxton & Rawls, 2005).

Relatively high NDVI values and large lag in the CPS 44 (Figure 9) coincide with a broad presence of Nitisols (55% of the area), which are characterized by deep horizons and clay contents higher than 30% (FAO, 2009). This favours moisture storage for longer periods of time (Bridges, 1997; Nicholson & Farrar, 1994). For CPS 7, the relatively short lag (Figure 8) corresponds with the presence of Leptosols (58% of the area) (FAO, 2009), which have more than 65% of sand content (Khan Towhid, 2013) that leads to short retention times. The relatively high NDVI peaks for CPS 37 (Figure 11) coincide with the presence of Cambisols (31% of the area), that have a loamy-clay texture and organic horizons with chemical composition that favours productivity (FAO, 2001). This finding confirms the effect of other soil properties in the NDVI-rainfall relationship (e.g. organic matter, soil fauna, nutrients, etcetera).

The Figures 8 to 11 indicate that the NDVI-rainfall relationship is approximately linear during the whole period of growing season (CPS 7, CPS 17, CPS 37), or only during a specific part (CPS 44). These results confirm the findings of Nicholson & Farrar (1994), who also identified that above a specific threshold *"the index saturates, and NDVI increases only very slowly with increasing rainfall or becomes constant"*. In this study, the observed saturation response is associated with rainfall amounts that do not limit crop growth, but otherwise relates with the effect of other environmental variables (Davenport & Nicholson, 1993).

5.2. Annual effective rainfall (CPS 7)

The linear annual relationship between the 10-day area-aggregate of NDVI and rainfall at the optimal lag explains 0.87 of the total variation in the NDVI values (Figure 12). The relationship also reveals high variability for the values during the last dekades of the growing season. This coincides with the previous finding about other factors that may have higher influence than rainfall during this period (section 5.1).

Problems regarding the annual NDVI-rainfall relationship are attributed to processes reducing the amount of effective rainfall (Doorenbos & Pruitt, 1977). The predictive power of the relationship at the last dekades however, does not notably improve after using fixed thresholds for rainfall to account for losses

due to evaporation and deep percolation (r-squared: 0.9) (Figure 13). Spatial aggregation of the rainfall at a CPS level, was assumed in this study as sufficient to remove the effect of runoff associated to the occurrence of localized extreme events (Grist et al., 1997).

Other factors affecting crop growth as assessed by NDVI in an area-aggregated level, include the effect by vegetation cover on evaporation (e.g. higher Eo with less green surface) (Doorenbos & Pruitt, 1977). This effect can be further considered through the use of differentiated thresholds for each stage of the growing season. The use of other explanatory variables to capture this effect is not advisable, because local variability as proved in section 4.3 can create additional uncertainty in estimating Eo losses (e.g. effect of radiation and temperature).

5.3. Agreement between seasonal negative NDVI and lagged rainfall anomalies (CPS 7)

Seasonal NDVI and lagged rainfall anomalies during the years 1999-2014 are estimated through the threshold method, which implies the calculation of the differences between the annual area-aggregated values and the median intra-annual profiles (including modifications to account for effective rainfall). For 13 out of 16 years evaluated, the seasonal negative NDVI anomalies coincide with the seasonal negative lagged rainfall anomalies in a general linear relationship (Figure 14). The development of this anomalies in the applicable growing season reflects major disagreements at the last dekades (Figure 15), which coincides with the stated problems in the NDVI-effective rainfall relationship (Section 5.2).

The assessment of the spatial agreement between seasonal negative NDVI and lagged rainfall anomalies (using the categories: very good, good, bad, very bad) is only 21.5% better than chance (Kappa coefficient). This result points out the difficulties to relate effective rainfall with agronomic drought at a pixel level and therefore the uncertainty of its aggregation at a CPS level. Dinku et al. (2014) and Osgood (2010) realizing similar exercises of validation in the Tigray region (CPS 7), also found limitations in the accurate representation of available water through the use of satellite estimates.

One of the factors that likely introduce more uncertainty in the validation is the existence of localized rainfall events that are not captured spatially and temporally by the satellite estimates of rainfall (Osgood, 2010). The infrared satellite products (e.g. CHIRPS) have problems in the collocation and estimation of rainfall when there are multi-cloud systems that interfere with the view of actual precipitation clouds, or the rainfall originates from warm clouds or orographic effects not detected using this technology (Tapiador et al., 2012). From the temporal perspective, the use of 10-day estimates of rainfall leaves out also the possibility to detect the occurrence of short drought events that occur at smaller scales or between the used dekadal periods.

The observed spatial variability can also be associated with other factors affecting local crop growth (e.g. temperature, radiation, wind, cloud coverage, diseases, etcetera) or available water (e.g. topography, farm management, soil porosity, etcetera) (Ceccato et al., 2008; Dinku et al., 2014). According to Boken (2005), the variables most important for crop growth are rainfall and temperature. In this study, rainfall is selected instead of temperature, because of its higher spatial variability that favours agronomic drought monitoring at a local level (Propastin et al., 2007). The availability of long term satellite estimates of rainfall (e.g. CHIRPS since 1981) also represents an advantage over operational satellite soil moisture products, which only provide estimates for the last 10 years (Petropoulos, Ireland, & Barrett, 2015). Potential advances of these technologies to assess soil moisture at great depths (e.g. below the 0-5 cm surface layer) might be an alternative to the use of satellite rainfall estimates in the future (Petropoulos et al., 2015).

5.4. Seasonal NDVI anomalies in relation to modelled soil moisture at a pixel level

In view of the difficulties experienced in this study to assess available water and the limitations that dekadal estimates of rainfall have in the detection of dry spells (section 5.3), the last part of this study consists of modelling daily soil moisture at a pixel level. In detail, soil moisture is estimated through the implementation of the Thornthwaite's water balance technique (1955), and the use of satellite derived daily estimates of rainfall (CHIRPS) and dekadal ETo (MARS-ECMWF).

The visual comparison of soil moisture estimates and NDVI anomalies in the years 2007-2010 (Figure 17), reveals that the agreement occurs at shorter time lags in the beginning of the growing season in comparison to the last dekades. Ji & Peters (2005), proved using distributed lag models to relate NDVI and rainfall, that the time lag relationship changes according to the stage of the growing season.

The high sensitivity of the NDVI anomalies to little amounts and poor distributed rainfall in the start of the growing season (2008, 2009, 2010) (Figure 17), can be associated to the occurrence of shallow roots and therefore high dependency on recent soil moisture (Ingram, 2005). It is observed for the middle and end of the growing season of the year 2007, that the poor distribution of rainfall does not show up in the current and subsequent NDVI anomalies (Figure 17). The same situation, visible in the last dekades of all years, can be related with a high or total dependence on previous soil moisture storage. According to Ji & Peters (2005), it is likely that an increase of rainfall in the end of the growing season does not have a relevant impact on vegetation growth, or instead affects it negatively (e.g. potential development of diseases). Allen, Pereira, Raes, & Smith, (1998), also confirm that an excess of rainfall *"will result in waterlogging which might damage the root and limit root water uptake by inhibiting respiration"*.

With regards to the model implemented, the main drawback relates to the unaccounted effects of probable runoff. Those effects can be triggered by frequent intense rainfall events reported in Ethiopia (e.g. average values around 20 mm/h in Mekele, capital of Tigray region) (Fazzini et al., 2015). The model, built under the assumption that all rainfall can potentially become soil moisture, leaves out the effect of other variables determining the real amount of water captured during intense rainfall events (e.g. infiltration capacity, existing moisture content in the top layer of the soil, vegetation cover and topography) (Citchley & Siegert, 1991). Considering that these factors cannot be accurately estimated at kilometer scale without the inclusion of other information, further improvement should be focus instead on the uncertainties of the used datasets.

The fact that CHIRPS is originally estimated in a pentad (5 days) and not daily scale might introduce uncertainty about the distribution of rainfall (Section 3.1.2) (Funk et al., 2015). Further validation studies of the CHIRPS daily algorithm will provide the support to confirm the limitations of the model implemented to identify short meteorological droughts, which can be devastating at some periods of crop growth (e.g. after seedling emergence) (Ingram, 2005).

The use of the MARS-ECMWF to simulate the evapotranspiration proccess is limited according to the dekadal resolution of the product. Further spatial and temporal improvements of this product will be helpful to include the effect of the vegetation cover on ETo (as discussed in section 5.2 in relation to Eo). However, the use of additional parameters might be introduced carefully, as already ETo estimates depends and accounts on the uncertainties of the measurements of wind, radiation, air temperature and humidity (Allen et al., 1998).

The main limitation of the NDVI is related with the mixture of vegetation covers that occur at the scale of the validation (5 km) or even at the original resolution of SPOT (1 km), which is not enough to separate the signal associated to the small farm sizes in Ethiopia (Anyamba, Tucker, Huete, & Boken, 2005; Dinku et al., 2009). A purposive selection of the pixels according to the extension of crop coverage might be helpful to refine the soil moisture model and its relationship with NDVI. Studies assessing the vegetative fraction in the NDVI signals can also be used to interpret crop growth development in mixed pixels (Dinku, 2014; Dinku et al., 2009).

6. CONCLUSIONS AND RECOMMENDATIONS

6.1. Conclusions

- The present study successfully derives the long term NDVI-rainfall relationships, which allow to analyze the macro-scale factors affecting the availability of water for vegetation development at a CPS level. The soil water holding capacity (dominated primarily by texture) is found to relate with the optimal time lag in each CPS, which vary between 5 to 8 dekades.

- The study verified that a saturation response occur in the annual NDVI-rainfall linear relationship of the CPS-7. This phenomenon attributed and corrected according to processes reducing the amount of effective rainfall did not notably improve the predictive power of the relationship during the end of the growing season. Consequently, the same problem was identified in the area-aggregate agreement between seasonal negative NDVI and lagged rainfall anomalies

- The simplified calculation of seasonal negative NDVI and lagged rainfall anomalies at a CPS level proved to agree for 13 out of 16 years evaluated. Spatial agreement of anomalies (Kappa coefficient of 21.5%) confirmed that this level of study still cannot be used in the practice as there are methodological limitations to represent local available water. In this sense, the attempt to model soil moisture at a daily level has been shown promising to include more detail about the distribution of rainfall and its effect in specific periods of the growing season.

6.2. Recommendations

- The explored method to derive effective rainfall uses fixed thresholds to mimic losses due to evaporation, but it does not consider the effect that vegetation cover has in this process through the growing season. A parametrization of this phenomenon in an area-aggregated level might improve the method. Further research on how the potential evapotranspiration products can be refined accordingly will help also in deriving more realistic soil moisture estimates than the obtained in the present study. Consequently, the development of potential sources to validate agronomic droughts as assessed by NDVI at a pixel level.

- The explored soil moisture model incorporates few assumptions and variables, but it does not report the reliability of the used methods and datasets to capture events affecting the crop growth at a daily level (e.g. distribution of rainfall, available water after an intense rainfall). Further studies incorporating a purposive selection of the pixels and ground information on previous events of drought, will be helpful to establish the effectiveness of the approach applied in this study.

7. LIST OF REFERENCES

Agricultural Transformation Agency. (2014). *Annual Report: Transforming agriculture in Ethiopia*. Retrieved from http://www.ata.gov.et/download/annual-report-transforming-agriculture-in-ethiopia/#

Allen, R. G., Pereira, L. S., Raes, D., & Smith, M. (1998). Crop evapotranspiration - Guidelines for computing crop water requirements. *FAO irrigation and drainage paper 56* (pp. 1–14). Rome, Italy: FAO.

Anyamba, A., Tucker, C., Huete, A., & Boken, V. (2005). Monitoring drought using coarse-resolution polar-orbiting satellite data. In *Monitoring and Predicting Agricultural Drought* (pp. 57–78). Oxford: Oxford University Press

Billi, P. (2015). Landscapes and landforms of Ethiopia. In P. Billi (Ed.), *Geomorphological landscapes of Ethiopia* (pp. 3–32). Dordrecht, The Netherlands: Springer.

Boken, V. (2005). Agricultural drought and its monitoring and prediction: some concepts. In *Monitoring and Predicting Agricultural Drought* (pp. 3–10). Oxford, United Kingdom: Oxford University Press.

Bridges, E. M. (1997). *World Soils* (3rd ed). Cambridge, United Kingdom: Cambridge University Press.

Ceccato, P., Brown, M., Funk, C., Small, C., Holthaus, E., Siebert, A., & Ward, N. (2008). *Technical issues in index insurance*. Retrieved from http://iri.columbia.edu/~deo/insurance_class_reading/Remote Sensing - Vegetation.pdf

Chuvieco, E., & Huete, A. (2010). *Fundamentals of Satellite Remote Sensing* (1st ed). Boca Raton, United States: Taylor & Francis Group.

Citchley, W., & Siegert, K. (1991). Rainfall-runoff analysis. In *Water harvesting*. Rome, Italy: FAO.

Davenport, M. L., & Nicholson, S. E. (1993). On the relation between rainfall and the Normalized Difference Vegetation Index for diverse vegetation types in East Africa. *International Journal of Remote Sensing*, *14*(12), 2369–2389. doi:10.1080/01431169308954042

de Bie, K. (2014). *The Micro Insurance Model*. Unpublished manuscript. Faculty of Geo-Information Science and Earth Observation, Enschede, The Netherlands.

Degefu, W. (1987). Some aspects of meteorological drought in Ethiopia. In M. Glantz (Ed.), *Drought and hunger in Africa denying famine a future* (pp. 23–36). Cambridge, United Kingdom: Cambridge University Press.

Dinku, T. (2014). Validation of the CHIRPS satellite rainfall estimate. Retrieved from ftp://ftp.chg.ucsb.edu/pub/org/chg/products/CHIRPS-2.0/pubs/mention-CHIRPS/Dinku.Validation_of_CHIRPS-poster.IPWG.Japan.2014.11.pdf

Dinku, T., Gianninni, A., Hansen, J., Holthaus, E., Ines, A., Kaheil, Y., … Vicarelly, M. (2009). *IRI Technical Report 09-04. Designing Index-Based Weather Insurance for Farmers in Adi Ha,Ethiopia*. Retrieved from http://iri.columbia.edu/resources/publications/pub_id/908/

Diro, G. T., Toniazzo, T., & Shaffrey, L. (2011). Ethiopian rainfall in climate models. In C. J. R. Williams & D. R. Kniveton (Eds.), *African Climate and Climate Change* (pp. 51–69). London, United Kingdom: Springer.

Dourado-Neto, D., Jong van Lier, Q. de, Metselaar, K., Reichardt, K., & Nielsen, D. R. (2010). General procedure to initialize the cyclic soil water balance by the Thornthwaite and Mather method. *Scientia Agricola*, *67*(1), 87–95. doi: 10.1590/S0103-90162010000100013

Doorenbos, J., & Pruitt, W. O. (1977). Crop water requirements. *FAO Irrigation and Drainage Paper No.24* Rome, Italy: FAO.

Eklundh, L. (1998). Estimating relations between AVHRR NDVI and rainfall in East Africa at 10-day and monthly time scales. *International Journal of Remote Sensing*, *19*(3), 563–570. doi:10.1080/014311698216198

ERDAS. (2003). *ERDAS Field Guide* (5th ed). Atlanta, United States: Erdas Inc. Retrieved from http://www.gis.usu.edu/manuals/labbook/erdas/manuals/FieldGuide.pdf

FAO//IIASA/ISRIC/ISS-CAS/JRC. (2009). Harmonized World Soil Database (version 1.1). Rome, Italy and IIASA, Laxenburg, Austria.

FAO. (2001). *Lecture notes on the major soils of the world.* In P. Driessen, J. Deckers, & F. Nachtergaele (Eds.). Rome, Italy: FAO.

Fazzini, M., Bisci, C., & Billi, P. (2015). The climate of Ethiopia. In P. Billi (Ed.), *Landscapes and landforms of Ethiopia* (pp. 65–87). Dordrecht, The Netherlands: Springer.

Funk, C., Peterson, P., Landsfeld, M., Pedreros, D., Verdin, J., Shukla, S., … Michaelsen, J. (2015). The climate hazards infrared precipitation with stations—a new environmental record for monitoring extremes. *Scientific Data*, *2*, 150066. doi: 10.1038/sdata.2015.66

Gebrehiwot, T., Van der Veen, A., & Maathuis, B. (2011). Spatial and temporal assessment of drought in the Northern highlands of Ethiopia. *International Journal of Applied Earth Observation and Geoinformation*, *13*(3), 309–321. doi: 10.1016/j.jag.2010.12.002

Gessner, U., Naeimi, V., Klein, I., Kuenzer, C., Klein, D., & Dech, S. (2013). The relationship between precipitation anomalies and satellite-derived vegetation activity in Central Asia. *Global and Planetary Change*, *110*, 74–87. doi: 10.1016/j.gloplacha.2012.09.007

Gommes, R., & Kayitakire, F. (2013). Overview: from early warning systems to index insurance. In R. Gommes & F. Kayitakire (Eds.), *The challenges of index-based insurance for food security* (pp. 9–14). Luxembourg, Luxembourg City: Publications Office of the European Union.

Grist, J., Nicholson, S. E., & Mpolokang, A. (1997). On the use of NDVI for estimating rainfall fields in the Kalahari of Botswana. *Journal of Arid Environments*, *35*(2), 195–214. doi:10.1006/jare.1996.0172

Herrmann, S. M., Anyamba, A., & Tucker, C. J. (2005). Recent trends in vegetation dynamics in the African Sahel and their relationship to climate. *Global Environmental Change*, *15*(4), 394–404. doi:10.1016/j.gloenvcha.2005.08.004

Hoscilo, A., Balzter, H., Bartholomé, E., Boschetti, M., Brivio, P. A., Brink, A., … Pekel, J. F. (2014). A conceptual model for assessing rainfall and vegetation trends in sub-Saharan Africa from satellite data. *International Journal of Climatology*, 3582–3592. doi: 10.1002/joc.4231

Hutchinson, C. F. (1991). Uses of satellite data for famine early warning in sub-Saharan Africa. *International Journal of Remote Sensing*, *12*(6), 1405–1421. doi: 10.1080/01431169108929733

Ingram, K. (2005). Drought-related characteristics of important cereals crops. In *Monitoring and Predicting Agricultural Drought* (pp. 11–27). Oxford: Oxford University Press.

Ji, L., & Peters, A. J. (2005). Lag and Seasonality Considerations in Evaluating AVHRR NDVI Response to Precipitation. *Photogrammetric Engineering & Remote Sensing*, *71*(9), 1053–1061. doi: 10.14358/PERS.71.9.1053

Khan Towhid, O. (2013). Problem Soils and their management. In *Soils. Principles, properties and management* (pp. 161–174). Dordrecht, The Netherlands: Springer

Lillesand, T., Kiefer, R. W., & Chipman, J. (2014). Digital image analysis. In *Remote Sensing and Image Interpretation* (7th ed, pp. 485–608). Hoboken, United States: John Wiley & Sons, Inc.

Maathuis, B., Mannaerts, C., Shouwenburg, M., Retsios, B., Lemmens, R., & Nkepu, M. R. (2014). *In Situ and Online Data Toolbox Installation, Configuration and User Guide*. Retrieved from http://52north.org/files/earth-observation/userguides/isod/ISOD_Toolbox_V1.4UG.pdf

Mishra, A. K., & Singh, V. P. (2010). A review of drought concepts. *Journal of Hydrology*, *391*(1-2), 202–216. doi: 10.1016/j.jhydrol.2010.07.012

Mishra, A. K., & Singh, V. P. (2011). Drought modeling - A review. *Journal of Hydrology*, *403*(1-2), 157–175. doi: 10.1016/j.jhydrol.2011.03.049

Nagarajan, R. (2010). Introduction. In R. Nagarajan (Ed.), *Drought Assessment* (pp. 1–27). New Delhi, India: Springer.

Nicholson, S., & Farrar, T. (1994). The influence of soil type on the relationships between NDVI, rainfall, and soil moisture in semiarid Botswana. I. NDVI response to rainfall. *Remote Sensing of Environment*, *50*(2), 107–120. doi: 10.1016/0034-4257(94)90038-8

Nicholson, S., Farrar, T., & Lare, A. (1994). The influence of soil type on the relationships between NDVI, rainfall, and soil moisture in semiarid Botswana. II. NDVI response to soil oisture. *Remote Sensing of Environment*, *50*(2), 121–133. doi: 10.1016/0034-4257(94)90039-6

Osgood, D. E. (2010). *HARITA IRI report to Oxfam America*. Retrieved from http://academiccommons.columbia.edu/catalog/ac%3A130677

Petropoulos, G. P., Ireland, G., & Barrett, B. (2015). Surface soil moisture retrievals from remote sensing: Current status, products & future trends. Physics and Chemistry of the Earth, Parts A/B/C, 83-84, 36–56. doi: 10.1016/j.pce.2015.02.009

Propastin, P. a, Kappas, M., Erasmi, S., & Muratova, N. R. (2007). Remote Sensing based study on intra-annual dynamics of vegetation and climate in drylands of Kazakhstan. *Basic and Applied Dryland Research*, *1*(2), 138–154. doi:10.1127/badr/1/2007/138

Reed, B. C., Brown, J. F., VanderZee, D., Loveland, T. R., Merchant, J. W., & Ohlen, D. O. (1994). Measuring phenological variability from satellite imagery. *Journal of Vegetation Science*, 5(5), 703–714. doi: 10.2307/3235884

Saxton, K. E., & Rawls, W. J. (2005). Soil water characteristic estimates by texture and organic matter for hydrologic solutions. *Soil Science Society of America Journal*, *70*(5), 1569–1578. doi: 10.2136/sssaj2005.0117

Stanimirova, R., Greatrex, H., Diro, R., McCarney, G., Sharoff, J., Mann, B., … Osgood, D. E. (2013). *Using Satellites to Make Index Insurance Scalable: Final IRI Report to the ILO Microinsurance Innovation Facility*. Retrieved from http://iri.columbia.edu/wp-content/uploads/2014/10/Using-Satellites-Scalable-Index-Insurance-IRI-ILO-report-2013.pdf

Tapiador, F. J., Turk, F. J., Petersen, W., Hou, A. Y., García-Ortega, E., Machado, L. A. T., … de Castro, M. (2012). Global precipitation measurement: Methods, datasets and applications. *Atmospheric Research*, *104-105*, 70–97. doi:org/10.1016/j.atmosres.2011.10.021

Udelhoven, T., Stellmes, M., del Barrio, G., & Hill, J. (2009). Assessment of rainfall and NDVI anomalies in Spain (1989–1999) using distributed lag models. *International Journal of Remote Sensing*, *30*(8), 1961–1976. doi:10.1080/01431160802546829

Van Loon, A. F., & Van Lanen, H. A. J. (2011). A process-based typology of hydrological drought. *Hydrology and Earth System Sciences Discussions*, *8*(6), 11413–11483. doi: 10.5194/hess-16-1915-2012

APPENDICES

Appendix A: Scientific model supporting the GIACIS project

According to de Bie (2014), the main technical considerations in the delineation of the Crop Production System zones are:

- Data: 10-day NDVI-images over the period May 1998-December 2013 (SPOT-VGT imagery, 1km2)
- Preprocessing: each image was geo-coded according the attached quality information. Then, the filter Savitsky-Golay was applied to remove residual noise caused by haze and clouds.
- Delineation of CPS: an unsupervised classification of the NDVI time-series was realized using the Iterative Self-Organizing Data Analysis Technique (ISODATA) (ERDAS, 2003). In detail the algorithm was applied 91 times varying the number of classes from 10 to 100. According to the divergence statistical measure of distance, the high average separability was found for 60 classes or CPS.
- Disaggregation of crop statistics by CPS: a stepwise forward linear regression was realized considering each CPS and the crop cultivated area statistics per Woreda/district (Agricultural Sample Enumeration/Census, CSA 2001/02). The correlation coefficients obtained explain between 60 to 75% of the variability. Specifically, the crops considered are: teff, wheat, barley, maize and sorghum (see statistics in Table 6).
- Selection of 24 CPS zones: according to its location in the highlands of Ethiopia (800 m.a.s.l), and percentages of crops above 5%.

Table 6. Percentage and type of crops cultivated in all delineated CPS

ID	Area (km²)	Teff	Wheat	Barley	Maize	Sorghum	Total
7	17722	4	4	3	0	4	16
10	16066	4	0	0	0	3	7
15	20104	10	5	4	0	0	19
16	17877	0	3	3	0	2	8
17	8193	0	0	0	3	3	6
18	18749	12	7	0	0	9	29
20	13517	9	0	0	10	7	26
22	22250	16	0	3	11	3	32
23	16717	0	7	12	12	0	31
25	13023	0	0	5	0	8	13
26	20627	0	0	0	2	4	6
29	17020	8	16	10	0	0	34
33	9964	9	0	0	0	8	17
36	14811	11	4	3	4	0	21
37	15010	0	0	0	5	5	9
38	15736	0	0	0	7	0	7
41	13376	6	0	4	8	0	18
42	8371	0	0	6	6	0	12
43	18565	0	4	0	4	7	15
44	14358	0	0	0	7	4	11
51	12802	11	7	7	11	4	39
57	12829	8	0	0	9	0	17
58	6253	0	0	0	11	0	11
59	9473	0	0	0	10	3	14

Appendix B: Soil map of Ethiopia

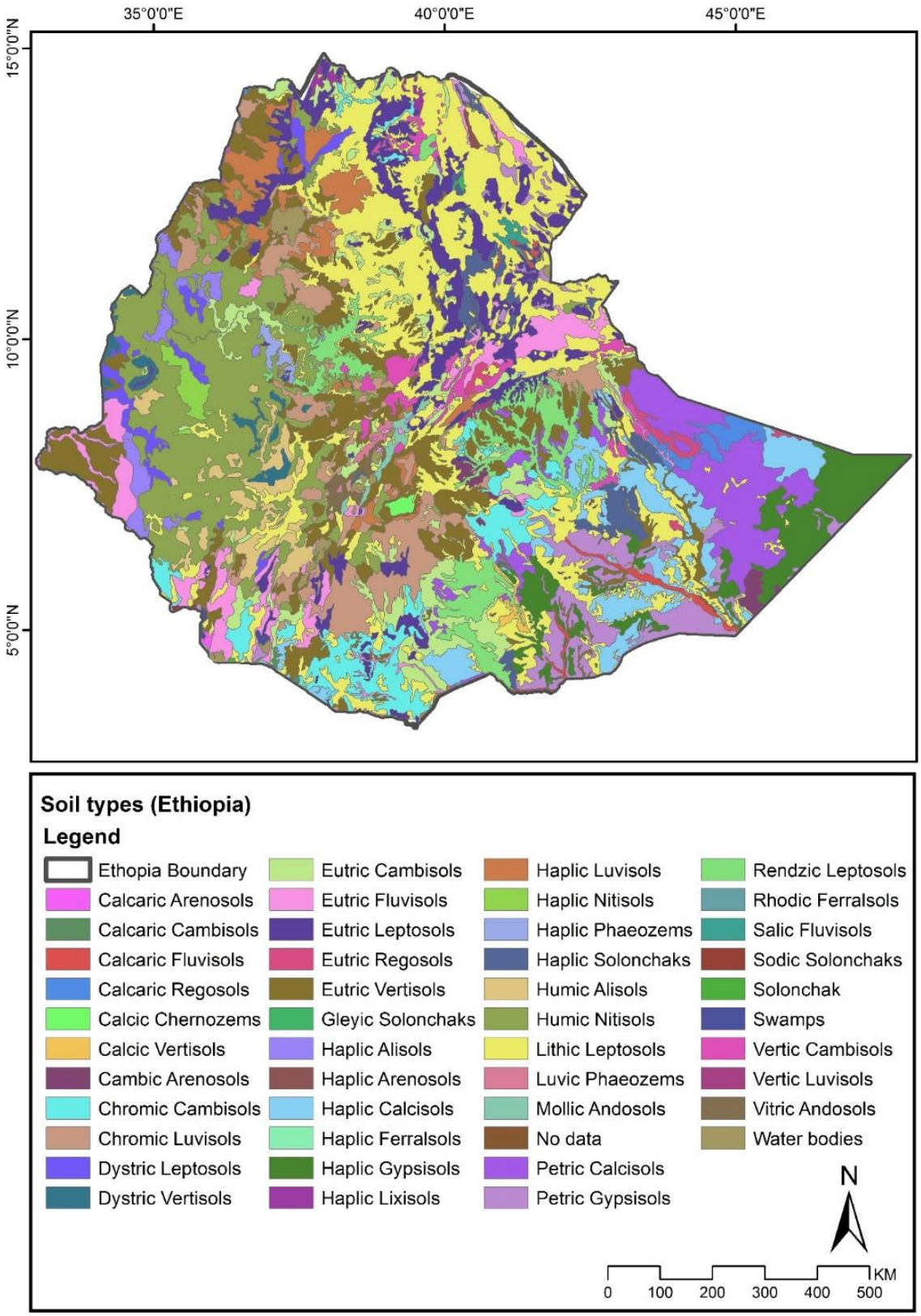

Figure 18. Soil map of Ethiopia

*Map produced according to the harmonized soil database of FAO (2009)

Appendix C: Spatial agreement of seasonal NDVI and lagged rainfall negative anomalies

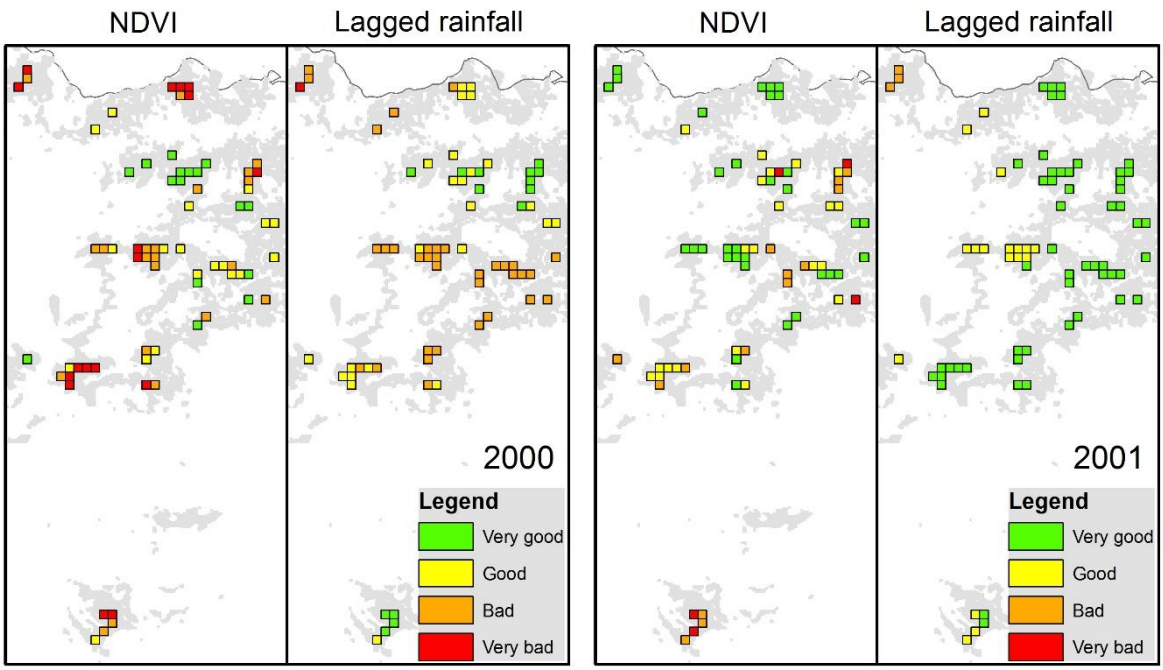

Figure 19. Spatial agreement of seasonal negative NDVI and lagged rainfall anomalies (2000 & 2001)

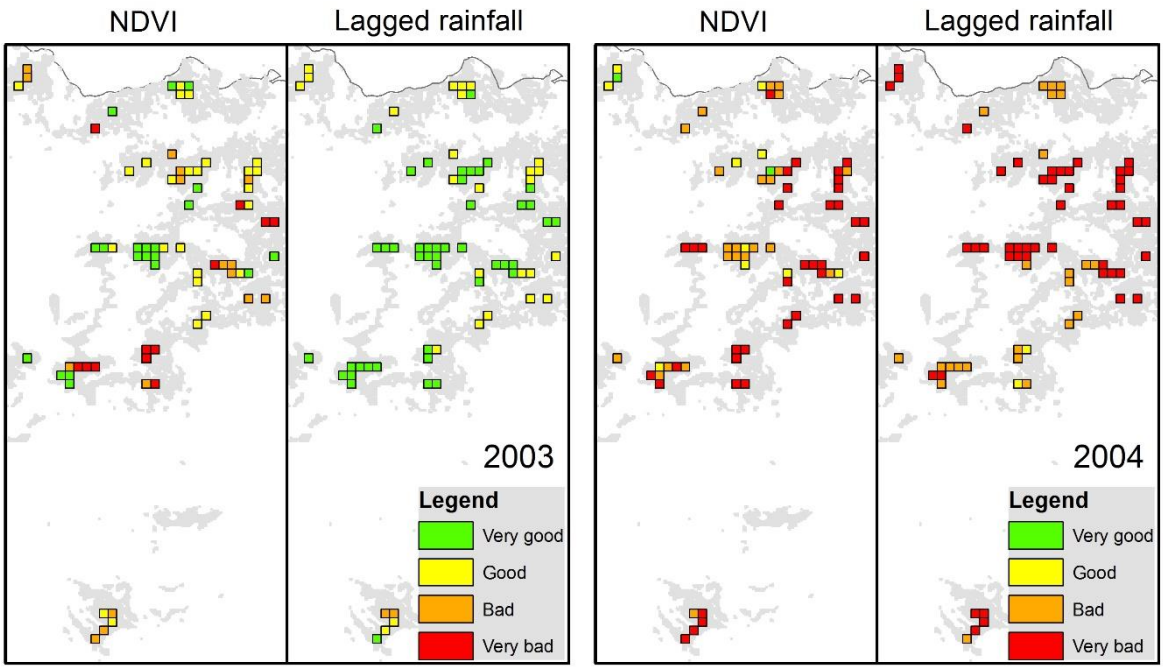

Figure 20. Spatial agreement of seasonal negative NDVI and lagged rainfall anomalies (2003 & 2004)

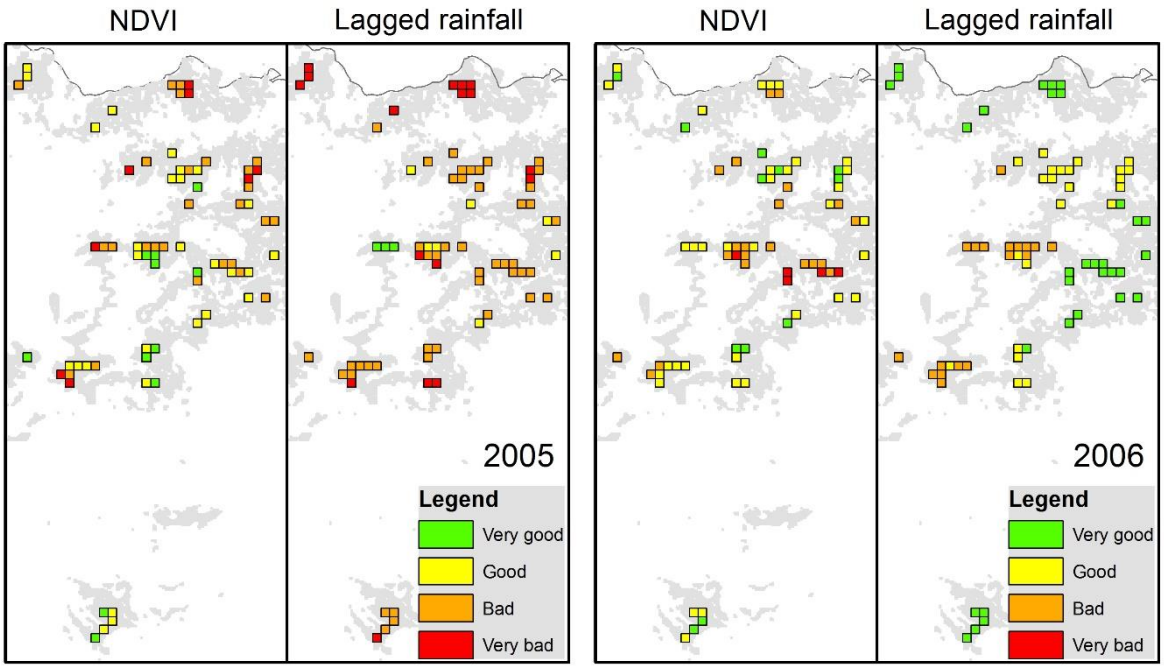

Figure 21. Spatial agreement of seasonal negative NDVI and lagged rainfall anomalies (2005 & 2006)

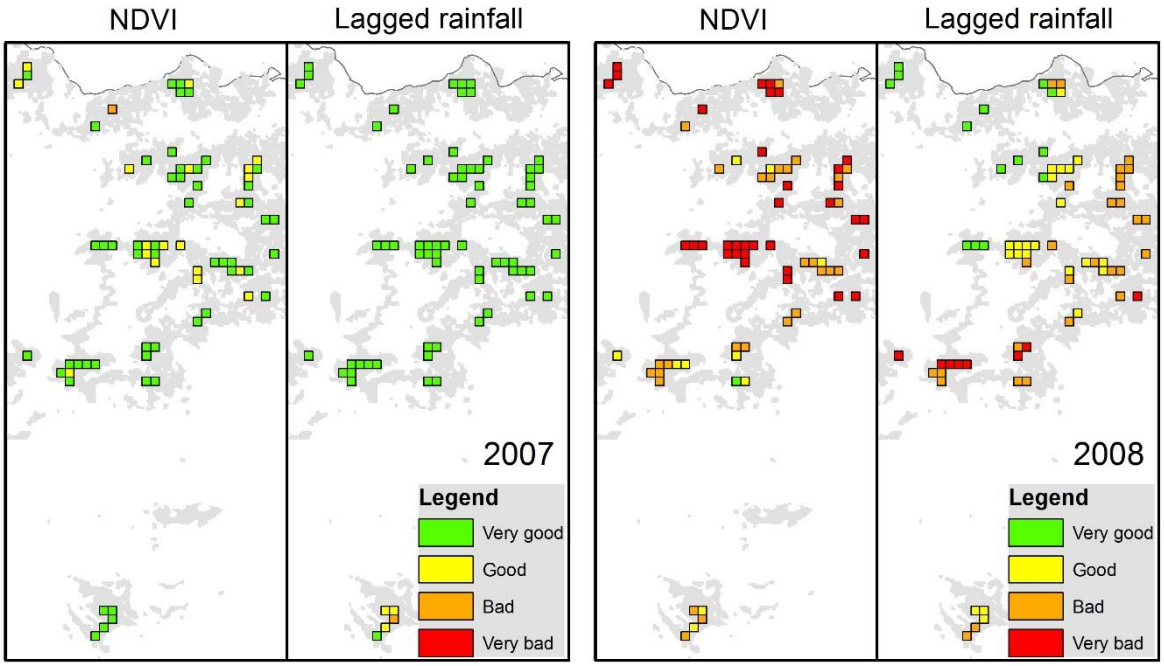

Figure 22. Spatial agreement of seasonal negative NDVI and lagged rainfall anomalies (2007 & 2008)

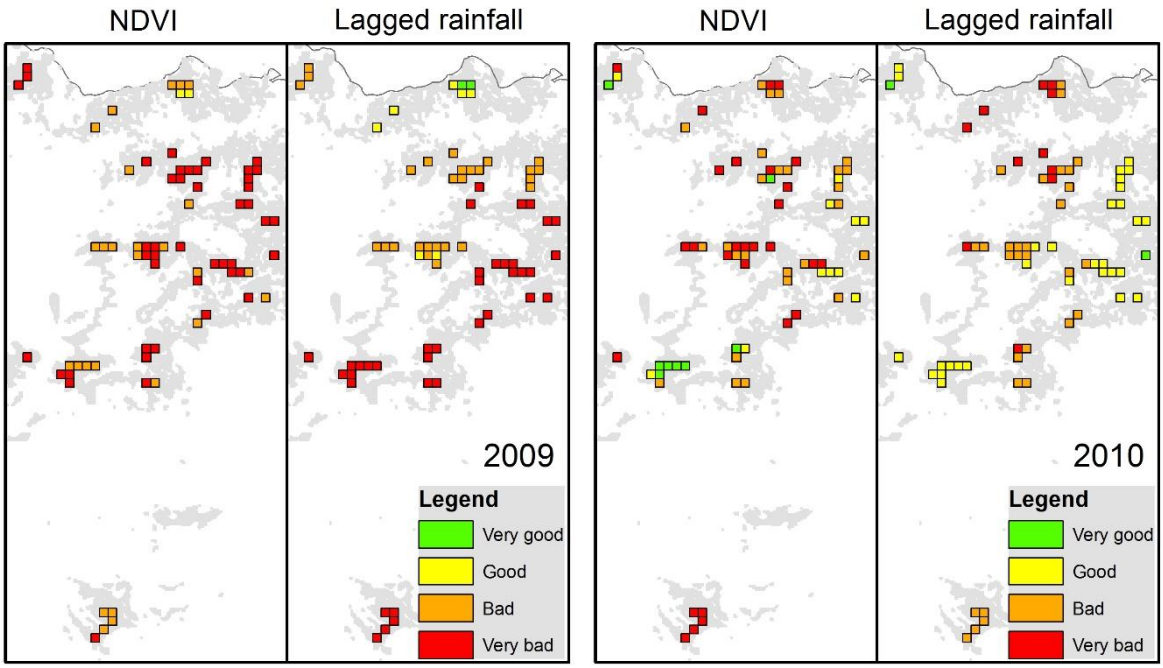

Figure 23. Spatial agreement of seasonal negative NDVI and lagged rainfall anomalies (2009 & 2010)

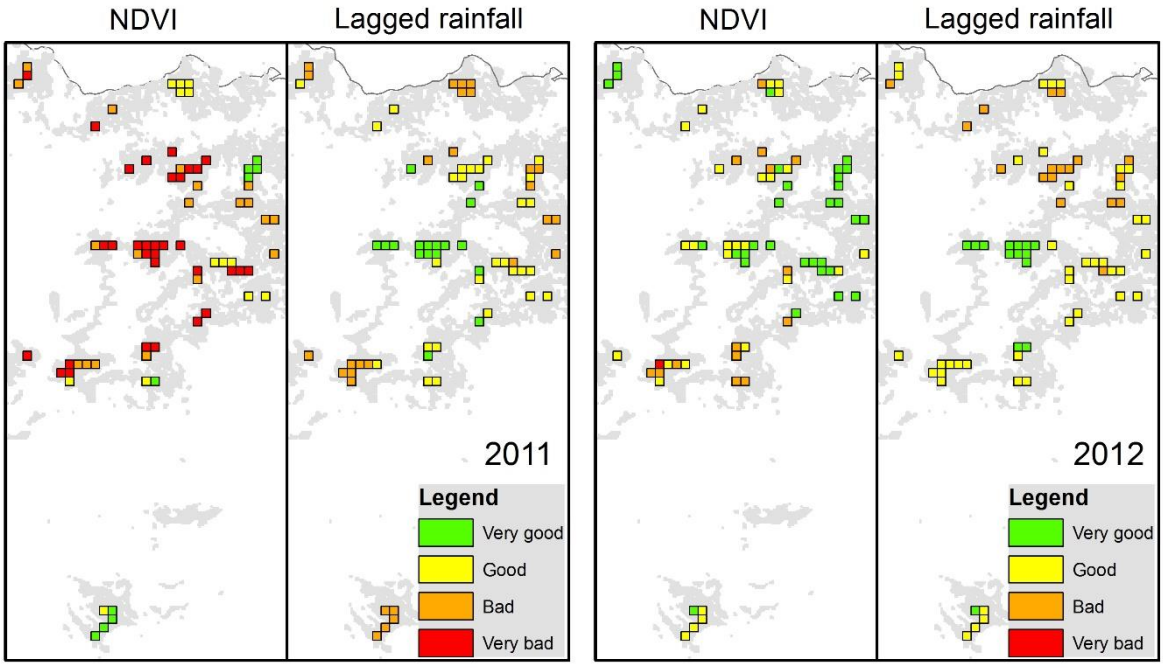

Figure 24. Spatial agreement of seasonal negative NDVI and lagged rainfall anomalies (2011 & 2012)

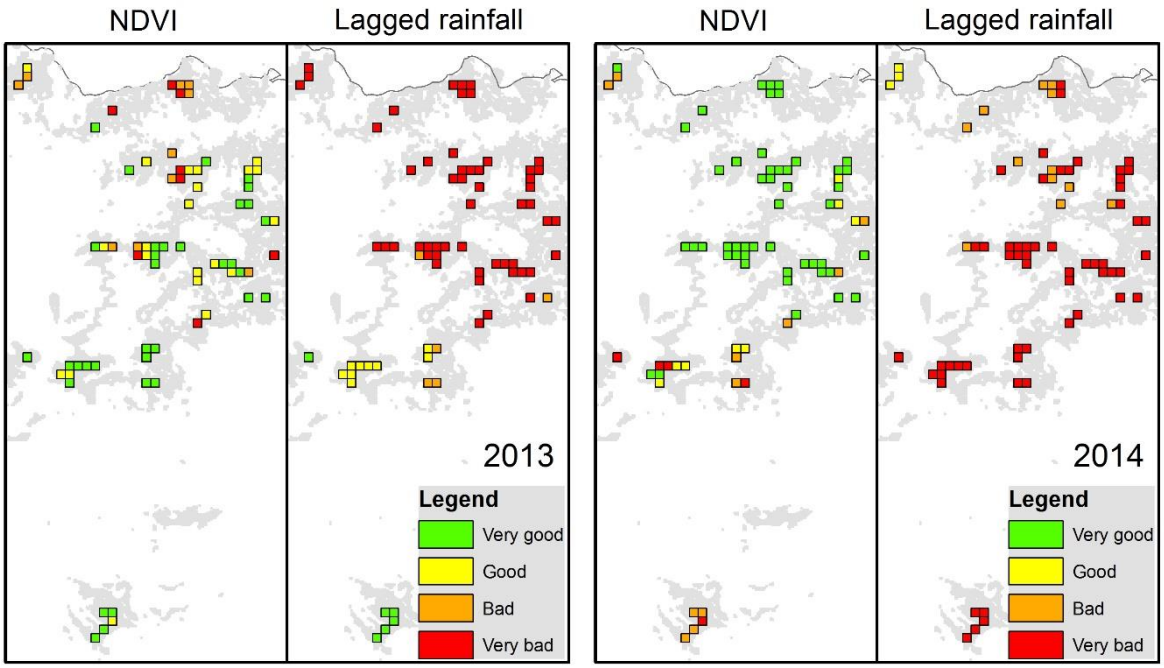

Figure 25. Spatial agreement of seasonal negative NDVI and lagged rainfall anomalies (2013 & 2014)

Appendix D: Soil moisture estimates within selected pixel in the CPS 7 (Tigray region)

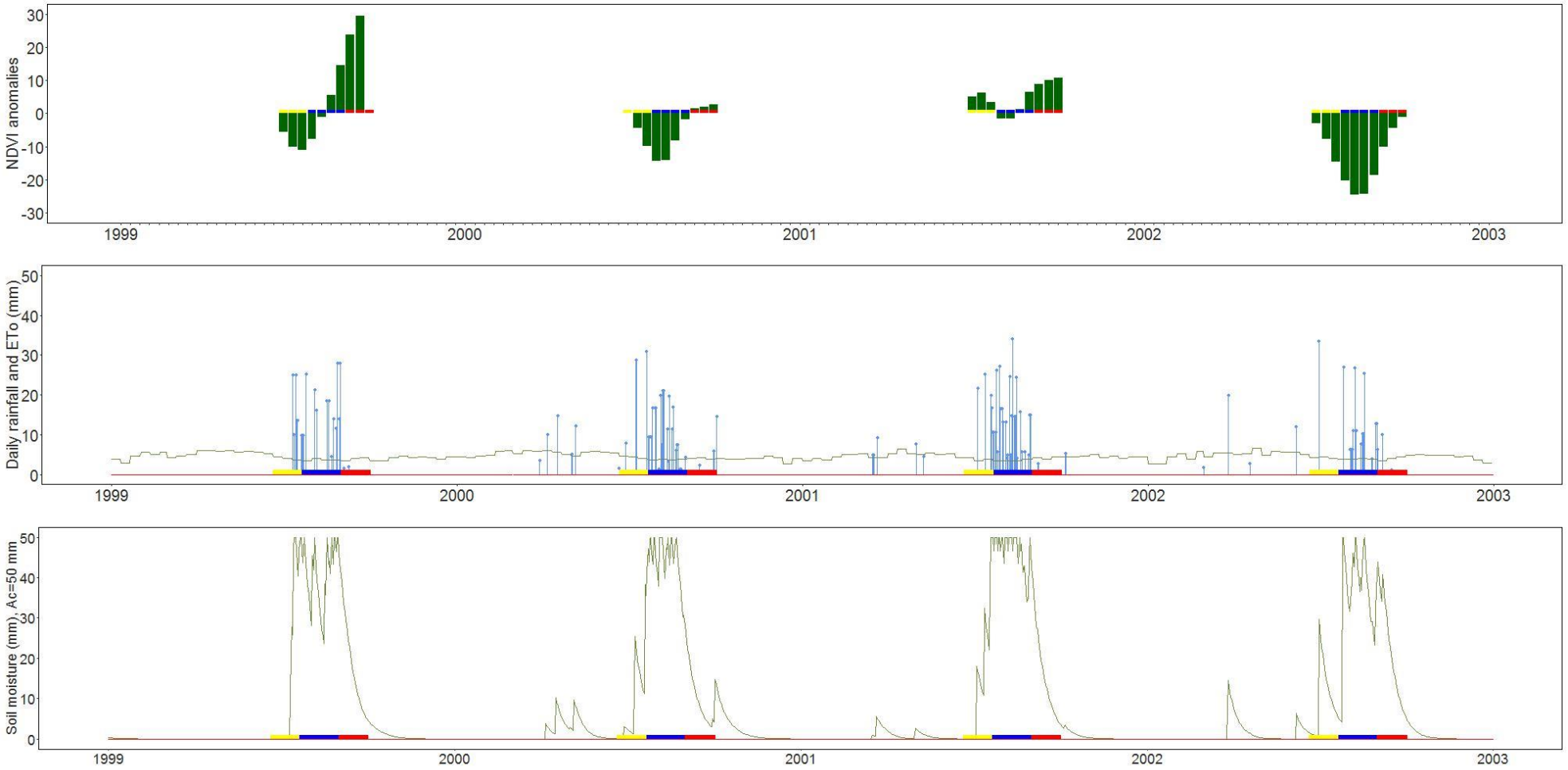

Figure 26.Soil moisture estimates within selected pixel in the CPS 7 (1999-2003)
The growing season appears divided in three segments, which corresponds to: beginning (yellow, 31 days), middle (blue, 41 days), end (red, 31 days)

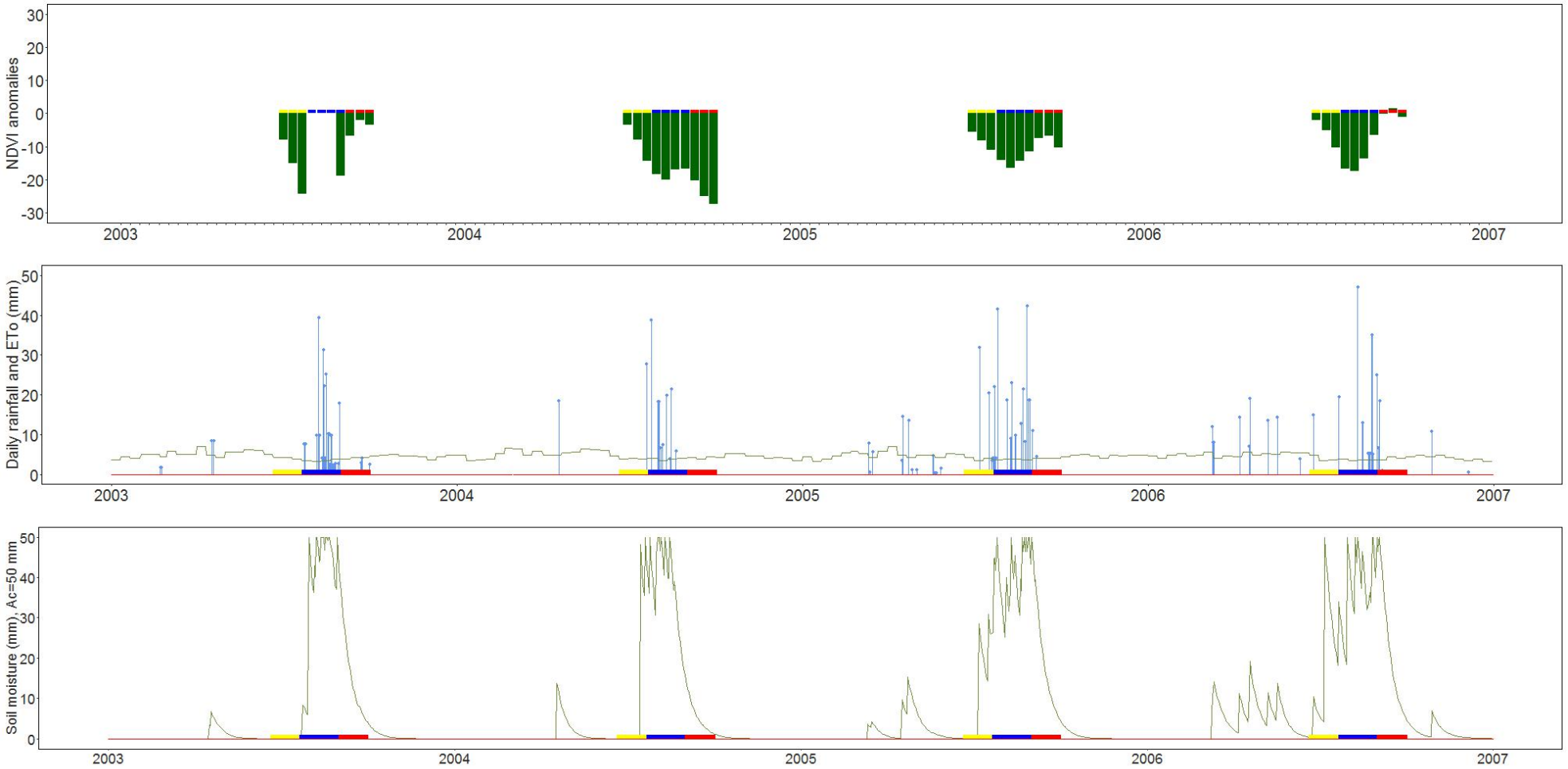

Figure 27. Soil moisture estimates within selected pixel in the CPS 7 (2003-2007)
The growing season appears divided in three segments, which corresponds to: beginning (yellow, 31 days), middle (blue, 41 days), end (red, 31 days)

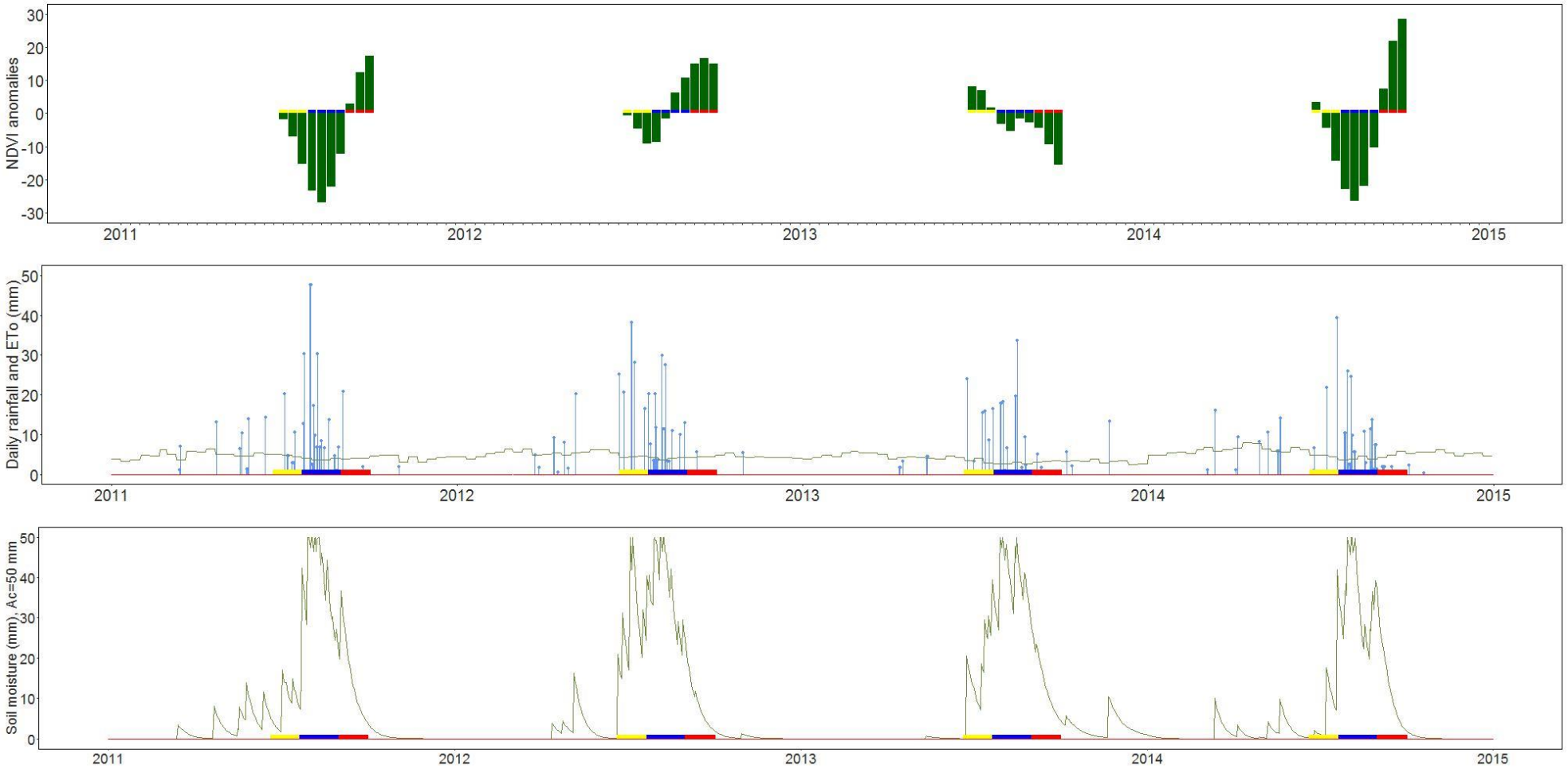

Figure 28.Soil moisture estimates within selected pixel in the CPS 7 (2011-2015)
The growing season appears divided in three segments, which corresponds to: beginning (yellow, 31 days), middle (blue, 41 days), end (red, 31 days)